rijksuniversiteit groningen

Bachelor Research Project

WBCE901-15

Biogas reforming in a membrane reactor

Author

Shi Wei Wu (s4048555)

Date

1st July 2022

Supervisor

Chelsea L. Tucker

Abstract

Reforming systems are thermodynamically limited by equilibria and require high temperatures to achieve a high yield. Membrane reactors can separate H_2 into pure streams using a H_2 selective membrane, thereby shifting the equilibria towards the product side. During this study the performance of a bi-reforming system model with and without a membrane was studied using Aspen Plus V1 and Aspen Plus Simulation Workbook Excel 2016. The performance was characterised with the H_2 and CO yield, the CH_4 and CO_2 conversion, and the reactor duty. The modelling was done using Gibbs energy reactors. The influence of operating conditions of the temperature, pressure, CH_4/CO_2 ratio, and the steam to carbon ratio were studied. The simulations showed that the base system without a membrane achieved a higher performance, as the membrane has a maximum operating temperature of 600°C, while the base system was not limited by the temperature. Therefore, the base system could be run at much higher temperatures.

1. Literature

1.1. Introduction

An over-reliance on fossil fuels have led to concerns such as depleting fuel sources, climate change, and pollution, resulting in a rising interest in clean, alternative fuels. One candidate for the role of alternative fuel is hydrogen. Currently, approximately 96% of the production of hydrogen is carried out using synthesis gas (syngas) (Minh et al. 2018). Syngas is a mixture of carbon monoxide (CO) and hydrogen (H_2) and is produced by reforming natural gas or oil (Rostrup-Nielsen 2000). It is used as an intermediate product in processes such as the Fischer-Tropsch synthesis, where it is converted into hydrocarbons (Dry 2002), methanation, or methanol synthesis

To be considered sustainable, hydrogen must originate from renewable sources. In this context, the utilization of biogas as a feed for syngas via reforming is of particular interest (Balagurusamy 2021). Biogas is formed by anaerobic digestion (AD) of organic material, often organic waste. As its main components consist of the greenhouse gases (GHG) carbon dioxide (CO_2) and methane (CH_4), the release of biogas, particularly methane which has a relative global warming potential of 72 compared to CO_2, into the atmosphere has negative effects on the environment (Parente et al. 2020; Scheutz et al. 2009). Currently, biogas is either converted into biomethane or used to generate electricity and heat through combustion. However, biogas combustion impacts the environment negatively in ways such as the release of CO_2 into the atmostphere, freshwater eutrophication and ecotoxicity (Ruiz et al. 2018). Utilisation of biomethane is associated with emissions of GHGs, albeit in low amounts (Scarlat et al. 2018). On the contrary, biogas reforming provides a pathway to turn these greenhouse gases into syngas and subsequently into clean and renewable fuels.

The four major reactions in biogas reforming are methane dry reforming (MDR), methane steam reforming (MSR), water-gas shift (WGS), and partial oxidation (PO) which are displayed in **equation (1)**, **(2), (3),** and **(4)** respectively (Parente et al. 2020; Rostrup-Nielsen 2000). Each reforming type has its own type of feed. The feed for dry reforming consists of biogas, for steam reforming of biogas and steam, and for tri reforming of biogas, steam, and oxygen (Zhao et al. 2020).

$$CH_4 + CO_2 \rightleftarrows 2CO + 2\,H_2 \quad (1)$$
$$CH_4 + H_2O \rightleftarrows CO + 3\,H_2 \quad (2)$$
$$CO + H_2O \rightleftarrows CO_2 + H_2 \quad (3)$$
$$CH_4 + \frac{1}{2}\,O_2 \rightleftarrows CO + 2\,H_2 \quad (4)$$

Additionally, side reactions may occur such as coke formation through methane decomposition (**equation (5)**) and the Boudouard reaction (**equation (6)**) (Parente et al. 2020; Rostrup-Nielsen 2000).

$$CH_4 \rightleftarrows C(s) + 2\,H_2 \quad (5)$$
$$2\,CO \rightleftarrows C(s) + CO_2 \quad (6)$$

The accumulation of coke on the catalyst surface can result in catalyst deactivation and plugging of the reactor. However, the process conditions can be altered such that coke formation is thermodynamically unfavoured, reducing the amount of coke formed during the process. Nickel is resistant to coke formation, readily available and has a lower price than noble metals, increasing its potential for this application.

1.2. Biogas

1.2.1. Biogas production

Anaerobic digestion of biomass is most carried out in landfills, digesters, and wastewater treatment plants. During anaerobic digestion, bacteria degrade organic matter in the absence of oxygen, during which CO_2 and CH_4 are produced. The feedstock of the biomass consists of organic waste, like animal manure, food waste, and crop residues. These feedstocks can be cheaply purchased from local farmers, while allowing them to generate additional income by selling waste (Sarker et al. 2018). However, this imposes a challenge related to the supply chain, as these farms are dispersed, leading to smaller scale reactors. Therefore, optimisation of the feedstock hub locations, transportation of the feedstock to the hubs, and site selection of the biogas reformers are vital to reduce capital and operating expenses (Sarker et al. 2018).

1.2.2. Biogas composition

Table 1 provides an overview of the biogas composition of various sources. The main components are given in volume percentage, as well as their impurities.

TABLE 1: OVERVIEW OF BIOGAS COMPOSITION.

Biogas source	CH_4 (%)	CO_2 (%)	N_2 (%)	O_2 (%)	H_2S (%)	Other	Reference
Organic raw materials	50-75	25-45	2	Trace	<1	H_2O: 2%-7% at 20-40 °C H_2: <1% Trace composites (e.g., NH_3, siloxane, and halides)	(Vita et al., 2014, as cited in Zhao et al. 2020)
Waste materials	50-70	25-50	-	-	-	-	(Yentekakis et al., 2015, as cited in Zhao et al. 2020)
Urban waste	40-70	30-60	-	-	-	-	(Zhang et al., 2015, as cited in Zhao et al. 2020)
	55-70	30-45	-	-	-	Some trace other gases	(Broun and Sattler, 2016, as cited in Zhao et al. 2020)
Biomass	55-70	27-44	-	-	<3	H_2: <1% Traces of siloxanes, NH_3, and halogenates	(Diez-Ramírez et al., 2016; Fei et al., 2016, as cited in Zhao et al. 2020)
Landfill gas	45-75	25-55	0-25	0.01-5	Trace	Trace composites (e.g., NH_3)	(Chen et al., 2017, as cited in Zhao et al. 2020)
	25-60	7-60	-	0.6-3	-	H2O: 3%-20% Trace amounts of other gases	(del Valle-Zermeño et al., as cited in Zhao et al. 2020)
	45-60	40-55	-	-	-	-	(Vita et al., 2015, as cited in Zhao et al. 2020)
	47-57	37-41	<1-17	<1	Trace	Benzene: 0.6-2.3 mg m^{-3} Toluene: 1.7-5.1 mg m^{-3}	(Rasi et al. 2007)
	59.4-67.9	29.9-38.6	n.a.	n.a.	Trace	Benzene: 21.7-35.6 mg m^{-3} Toluene: 83.3-171.6 mg m^{-3}	(Shin et al., 2002, as cited in Rasi et al. 2007)
	37-62	24-29	n.a.	<1	n.a.	Benzene: <0.1-7 mg m^{-3} Toluene: 10-287 mg m^{-3}	(Allen et al., 1997, as cited in Rasi et al. 2007)
	55.6	37.14	n.a.	0.99	n.a.	Benzene: 3.0 mg m^{-3} Toluene: 55.7 mg m^{-3}	(Eklund et al., 1998, as cited in Rasi et al. 2007)
	44	40.1	13.2	2.6	Trace	Toluene: 65.9 mg m^{-3}	(Jaffrin et al., 2003, as cited in Rasi et al. 2007)
	35-65	15-50	5-40	0-5	Trace	NH_3: trace amounts	(Minh et al. 2018)
Sewage digester	61-65	36-38	<2	<1	<0.1 ppm	Benzene: 0.1-0.3 mg m^{-3} Toluene: 2.8-11.8 mg m^{-3}	(Rasi et al. 2007)
Farm biogas plant	55-58	37-38	<1-2	<1	Trace	Benzene: 0.7-1.3 mg m^{-3} Toluene: 0.2-0.7 mg m^{-3}	(Rasi et al. 2007)

Table 1 shows that CH_4 and CO_2 form the bulk of the biogas in each scenario. However, the biogas compositions vary between different biogas sources and even within the same source category. A significant amount of nitrogen (N_2) is present in biogas from landfill gas, which acts as an inert gas (Zhao et al. 2020). Its presence leads to higher energy consumptions if it is not removed. Purification of the biogas is required before the reforming process, as the biogas

contains small amounts of impurities, such as NH_3, H_2S, aromatics and siloxanes (Zhao et al. 2020). These siloxanes lead to damage to the biogas reforming reactors and generate toxic emissions, limiting the application of biogas. H_2S is an impurity that can lead to catalyst deactivation and corrosion of equipment, at very low concentrations (Gao et al. 2018).

1.3. Biogas dry reforming

During the dry reforming process, CH_4 and CO_2 are converted into syngas which proceeds according to equation **(1)**. As the reaction is endothermic, increasing the temperature will allow for higher conversions. The H_2 and CO are obtained in a 1:1 ratio, therefore, additional H_2 is required to use the syngas in processes such as Fischer-Tropsch or the synthesis of methanol (Rasi et al. 2007).

Common side reactions consist of the reverse water-gas shift reaction (RWGS), coke formation, and the Boudouard reaction, given in **equations (3)**, **(5)**, and **(6)** respectively. The RWGS reaction results in a lower conversion of CH_4 compared to CO_2.

The accumulation of coke on the catalyst surface can result in catalyst deactivation and plugging of the reactor. Nickel is resistant to coke formation, readily available and has a lower price than noble metals, increasing its potential for this application. It was found that methane decomposes at temperatures above 533°C and that the Boudouard reaction occurs when the temperature is lower than 700°C (Gao et al. 2018). Therefore, it can be concluded that coke formation will prominently occur at temperatures between 533°C and 700°C, although it is not negligible at temperatures past 700°C. In contrast to increasing the temperature, increasing the pressure decreases the yield of H_2 and the conversion of CH_4 (Minh et al. 2018). Additionally, increasing the temperature will also lead to a higher energy consumption, directing attention at low-temperature (<700°C) dry reforming (Minh et al. 2018).

For a biogas dry reforming process at a temperature of 300°C, it was found that a 60% and 50% conversion for CH_4 and CO_2 could be reached respectively. This indicates that the production of H_2 by means of dry reforming is thermodynamically possible at lower temperatures. (Wang et al. 2018).

Ni-based catalysts are typically used for dry reforming due to their low cost; however, several problems arise with the usage of Ni-based catalysts. Firstly, low activity was found with existing Ni-catalysts. Secondly, due to the formation of nickel monoxide (NiO) shells on the catalyst, the catalyst deactivates quickly. Thirdly, formation of coke causes the catalyst to deactivate more rapidly. (Wang et al. 2018).

1.4. Biogas bi-reforming

Bi-reforming is the combination of dry reforming and steam reforming (equation **(1) and (2) respectively**). Subsequently, the CO is used in the WGS reaction to form more H_2. Like dry reforming, biogas steam reforming is carried out at high temperatures, around 800°C (Matsumura and Nakamori 2004). The process suffers from the same disadvantages as dry reforming such as the use of temperature-resistant materials and a high energy consumption. With the latter in mind, research is done on low-temperature to reduce the energy intensity of the process (Zhao et al. 2020).

Low-temperature reforming allows for milder operating conditions, though the operating temperature is still relatively high. Conventionally, the temperature range is between 400°C and 600°C, requiring less energy to operate and allowing the reactors to be powered by heat recovery utility (Angeli et al. 2014). Furthermore, cheaper materials that are less temperature-

resistant can be used for the reactor tubing. However, in exchange for these advantages, the H_2 yield is compromised due to thermodynamic limitations.

In contrast to dry reforming, coke formation is inhibited by the presence of steam. Furthermore, removal of any H_2O present in the biogas is not required. Whilst nickel catalysts are also widely used for bi-reforming, noble metals were found to be more active and more resistant to poisoning, however their high cost prevented them from being applied in large-scale processes (Kumar et al. 2015).

1.5. Tri reforming

The addition of PO to bi-reforming results in tri reforming. The reaction equation of PO is displayed below in **equation (4)** (Zhao et al. 2020). Like in bi reforming, coke formation can be inhibited, however the O_2 in the tri reforming system can help inhibit the formation even further (Zhao et al. 2020). In addition, O_2 can promote exothermic side reactions, which decreases the endothermicity of the process. However, careful monitoring is required to avoid hotspots in the reactors (Zhao et al. 2020). As the O_2 content in biogas is low, additional O_2 may be required, making the process more expensive. Furthermore, O_2 can oxidise the Ni catalysts, leading to catalyst deactivation.

1.6. Limitations of bi and tri reforming

As stated before, the endothermic nature of the bi and tri reforming reactions prevent high H_2 yields from being achieved at lower temperatures. Therefore, traditional reforming systems are run at temperatures above 700°C, intensifying the energy requirement of the process. Additionally, the H_2 production is further limited by the thermodynamic equilibrium of the reactions.

1.7. Membrane reactors

The limitations of bi and tri reforming may be overcome by using membrane reactors (Soria et al. 2019). Membrane reactors contain a selective membrane that continuously allows certain compounds to pass through. By removing H_2 through a H_2 selective membrane, the reaction equilibrium is shifted towards the reaction products.

The H_2 is separated through the membrane into the permeate stream, while the remaining reaction products form the retentate stream. The membrane must have the following characteristics: high selectivity towards H_2, high flux, high mechanical and chemical stability, and ideally low cost (Gallucci et al., 2013). The membranes can be divided in categories depending on the material on construction. Table 2 provides an overview of different membrane types and their properties, materials, transport mechanisms, and cost indications.

As shown in Table 2, dense polymer membranes can be operated at temperatures up to a 100°C. However, according to Gallucci et al. (2011), polymeric membranes can resist temperatures up to 300°C. Despite the increased temperature range, this temperature is still not sufficiently high enough to be used in a reforming process. Additionally, polymeric membranes possess a low selectivity towards H_2 and a low flux, as well as stability and poisoning issues.

Metal membranes are made from dense metals and can operate at higher temperatures up to 300 to 600°C. Palladium (alloys) were found to be highly selective and permeable to hydrogen gas. However, due to its rarity, pure palladium membranes are expensive (Gallucci et al. 2011). As a solution, a palladium coating is applied to a ceramic membrane, decreasing the cost to

manufacture the membrane. Alternatively, other dense metals such as tantalum, vanadium, or nickel can be used. In addition to high cost, metal membranes are prone to surface poisoning. Gases such as H_2S and CO are absorbed on the surface. However, the membrane is not permeable to H_2S and CO, decreasing the amount of dissociation sites for H_2.

TABLE 2: OVERVIEW OF MEMBRANE TYPES USED IN HYDROGEN SEPARATION. DATA TAKEN FROM KLUITERS (2004).

Parameter	Dense polymer membranes	Dense metallic membranes	Micro porous ceramic membranes	Dense ceramic membranes	Porous carbon membranes
Temperature range	<100°C	300-600°C	200-600°C	600-900°C	500-900°C
H_2 selectivity	Low	>1000	5-139	>1000	4-20
H_2 flux (10^{-3} mol/m^{2}s) at dP=1 bar	Low	60-300	60-300	6-80	10-200
Stability issues	Swelling, compaction, mechanical strength	Phase transition	Stability in H_2O	Stability in CO_2	Brittle, oxidising
Poisoning issues	HCl, SO_x, CO_2	H_2S, HCl, CO	-	H_2S	Strong adsorbing vapours, organics
Materials	Polymers	Palladium alloys	Silica, alumina, zirconia, titania, zeolites	Proton conducting ceramics (mainly $SrCeO_{3-\delta}$ and $BaCeO_{3-\delta}$)	Carbon
Transport mechanism	Solution / diffusion	Solution / diffusion	Molecular sieving	Solution / diffusion (proton conduction)	Surface diffusion; molecular sieving
Cost	Low	Low	Low	Low	Moderate

Ceramic membranes are constructed from aluminium, titanium, or silica oxides. They are resistant to high temperatures and poisoning. However, they are difficult to seal in reactors operating at a high temperature and susceptible to temperature gradients, which leads to membrane cracking (Gallucci et al. 2011).

To attain high conversions at temperatures below 700°C, a high differential pressure is required. However, the reforming reactions are thermodynamically unfavoured at increased pressures, thereby increasing the energy consumption of the system. At lower pressures, the driving force may be increased by applying a vacuum on the permeate side of the membrane. Alternatively, the use of protonic membranes may offer a solution (Kyriakou et al. 2016). The feed is fed over an electro-catalyst, the anode, where the reforming process occurs. At the anode, the produced H_2 is converted into protons and transported through an electrolyte to the cathode. At the cathode, the protons are converted into H_2 gas (Kyriakou et al. 2016). Through this method, the use of higher pressures and palladium is not required.

1.8. Hypothesis and key questions

The hypothesis was formulated as follows; A high H_2 separation factor of the membrane leads to an increased performance in a bi reforming system. The performance of the system was defined by the H_2 and CO yield, the CH_4 and CO_2 conversion, and the duty. The relevant key questions were identified as:

- What are the ideal operating conditions of a bi reforming system without a membrane?
  - How does the temperature affect the performance of the system?
  - How does the pressure affect the performance of the system?
  - How does the feed composition affect the performance of the system?
- Is the equilibrium shift caused by the removal of H_2 under high pressure sufficient to justify the lower conversions?

2. Method

2.1. Base case model

A simple base case model was built using Aspen Plus V11 and Aspen Plus Simulation Workbook Excel 2016 to determine the optimal operating conditions of a bi-reforming system. Initially, the performance of a tri-reforming system without a membrane was also studied, however it was found that it was outperformed by the bi-reforming system in terms of H_2 production. The results for the tri-reforming system can be found in the Appendix. The model consisted of a single reactor block connected to an in- and output stream. The reactor was modelled with a Gibbs energy reactor (RGibbs), which identifies the product composition for which the products have a minimal Gibbs free energy under the reactor's operating conditions. The feed consisted of CH_4, CO_2, and H_2O with a constant total flow of 1 kmol/h.

Scenario tables connected to the Aspen Plus model were created in Aspen Plus Simulation Workbook Excel 2016. Table 3 provides an overview of the relevant input variables and the range over which they were tested. Simulations were run for changing reactor temperatures and pressures, and for varying feed compositions.

The performance of the system was assessed by the conversion of CH_4 and CO_2 (X_{CH4} and X_{CO2}), the yield of H_2 and CO (Y_{H2} and Y_{CO}), and duty of the system. The definition of the conversions and yields can be found in **equations (7-10)**, where $F_{CH_4,feed}$ and $F_{CO_2,feed}$ denote the molar flowrates of CH_4 and CO_2 in the feed respectively.

TABLE 3 – RANGE OF VARIABLES STUDIED

Variable	Range
Temperature	300 - 900°C
Pressure	1 - 20 bar
CH_4/CO_2 ratio	1 - 3
H_2O/carbon ratio	0 - 1.5

Under certain reaction conditions the WGS reaction may become more prevalent. As a result, CO is used to form more H_2 causing the H_2 yield to increase and potentially exceed 100%. Additionally, a negative CO_2 conversion can be obtained due to the WGS reaction, as CO_2 is produced during this process.
The yields and conversions were calculated for each simulation case from the obtained flow rates, as well as the duty of the bi-reforming system.

$$X_{CH_4}(\%) = \frac{F_{CH_4,feed} - F_{CH_{out}}}{F_{CH_4,feed}} * 100\% \quad (7)$$

$$X_{CO_2}(\%) = \frac{F_{CO_2,feed} - F_{CO_{2out}}}{F_{CO_2,feed}} * 100\% \quad (8)$$

$$Y_{H_2}(\%) = \frac{F_{H_2,out}}{F_{CH_4\,feed} + F_{CO_2 feed}} * 100\% \quad (9)$$

$$Y_{CO}(\%) = \frac{F_{CO,out}}{F_{CH_4,feed} + F_{CO_2,feed}} * 100\% \quad (10)$$

2.2. Membrane model

2.2.1. Approximating membrane reactors

Aspen Plus does not possess a unit operation for the continuous removal of a compound in a membrane reactor. Therefore, the process was approximated using a series of alternating sub-reformers and sub-reactors. The basis of this method was a study done by Parente et al. (2020). Overall, the model consists of $(n + 1)$ sub-reformers and n sub-separators, and using a constant feed flow rate of 1 kmol/h. A system where $n = 1$ consists of 1 separator and 2 sub-reformers. For $n = 0$, the system would correspond to the base case model, as there are zero separators in this case. A schematic overview of the system is provided in figure 1. The outlet of the n^{th} sub-reactor is fed to the n^{th} sub-separator. The permeate stream consists of pure H_2 and is removed from the syngas in each sub-separator. The retentate stream flowing out of the n^{th} sub-separator is then fed to the $(n + 1)^{th}$ sub-reactor. The total permeation capacity of the membrane is divided over n sub-separators.

A larger number of sub-reformers and sub-separators are required to accurately model the continuous removal of H_2 through the membrane. Ye et al. (2009) found that the production rate of hydrogen did not depend on n for $n > 50$. For this study, the following values of n were compared: 0, 1, 2, 5, 10, 50.

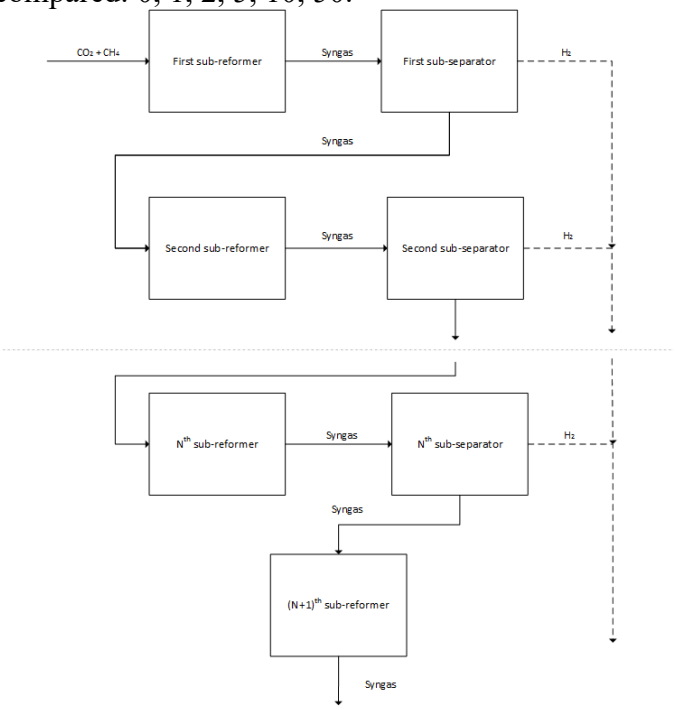

Figure 1: Schematic overview of a bi-reforming system with n sub-reformers, method adapted from Parente et al. (2020).

2.2.2. Determining the membrane properties

The total permeation capacity of the membrane in the simulation is dependent on the membrane flux. The definition of the membrane flux (J_i) is shown in **equation (11)**, where P_i is the permeability, A the membrane area, ΔP the pressure difference between the retentate and permeate side of the membrane, and l the membrane thickness (Edlund et al., 2010). The permeating gas, in this case H_2, is denoted with the subscript i.

$$J_i = P_i A \frac{\Delta P}{l} \tag{11}$$

To calculate the flux the membrane area, thickness, and permeability must be known. Table (4) provides an overview of the membrane properties and the feed flow rate that were used in an experimental study by Gallucci et al. (2004). This study covered a reforming reaction in a small-scale membrane reactor. A feed flow rate of 7,29 mL/min, or 0,0182 mol CH_4/min, and a membrane area of 5.3 cm^2 were used during this experiment. The thickness of the membrane was 50 µm.

TABLE (4) – PROPERTIES OF THE MEMBRANE THAT WAS USED DURING THE CALCULATIONS

Parameter	Value	Source
Area	5.3 cm^2	(Gallucci et al., 2004)
Thickness	50 µm	(Gallucci et al., 2004)
Flow rate	7,29 mL CH_4/min	(Gallucci et al., 2004)
Permeability	33500 Barrer	(Yun & Oyama, 2011)

The membrane must be upscaled to attain a sufficient permeation capacity for the feed flow rate of the model. Therefore, the area to feed ratio was calculated from the data in Table (4):

$$\frac{A}{F_{CH4} * 60} = \frac{5.3\ cm^2}{0.0182\ \frac{mol}{min} * 60 \frac{min}{hr}} = 291.5 \frac{cm^2}{mol * hr} = 291.5 * 10^3 \frac{cm^2}{kmol * hr}$$

Using a feed flow rate of 1 kmol/h results in an area of 291.5*10^3 cm^2. The permeability in Table 4 was taken from a different study, as it was not available in Gallucci et al. (2004). Then, having found a value for the membrane area, permeability, and thickness, the pressure difference was used as a variable. The total flux was divided over the number of sub-separators in the model. The calculated fluxes are displayed in Table 5. As visible in the Table 5, the flux increases with increasing pressure differences, as it is the driving force.

TABLE 5 – THE CORRESPONDING FLUX OF EACH PRESSURE DIFFERENCE

ΔP (bar)	Flux (mol/h)
1	31,4
5	157
10	314

2.3.3. Setting up the model

A model was setup in Aspen Plus to model the membrane reactor. A scenario table was created to enter all the relevant inputs. The model was setup as shown in Figure 1, with 1, 5, 10, or 50 separators blocks depending on the value of n. Each sub-separator had a H_2 flux equal to the total capacity divided by n.

Each Gibbs reactor block was run at a temperature range of 300 to 600°C at a pressure difference of 1, 5, and 10 bars. It was assumed that the permeate side of the membrane was under atmospheric pressure, thus the Gibbs reactors were run at 2, 5, and 11 bars respectively. The feed had a flow rate of 1 kmol/h and contained 60% H_2O, 20% CH_4, and 20% CO_2.

From the results, the H_2 and CO yields and the CH_4 and CO_2 conversions were calculated using **equations (7-10)**. Additionally, the duty of each reactor was taken.

3. Results

3.1. Base case model

3.1.1. Effect of temperature and pressure

The H_2 yield at varying operating pressures was plotted against the temperature to study the effect of temperature and pressure. The feed consisted of 1 kmol/h with a 0.5 mole fraction for both CH_4 and CO_2. Figure 2 shows that the H_2 yield increases with an increasing temperature, as expected given the endothermic nature of the system. Additionally, it was confirmed that increasing the pressure negatively affects the H_2 yield. Identical trends were found for the CH_4 and CO_2 conversions, the CO yield, and the duty of the system. The figures of which can be found in appendix A-1, A-2, A-3, and A-4 respectively. An increase in conversion, yield, and duty can be found for an increasing temperature, as the reactions are favoured and thus the equilibrium is shifted towards the products. The inverse behaviour was observed for an increase in pressure, as the reactions are inhibited.

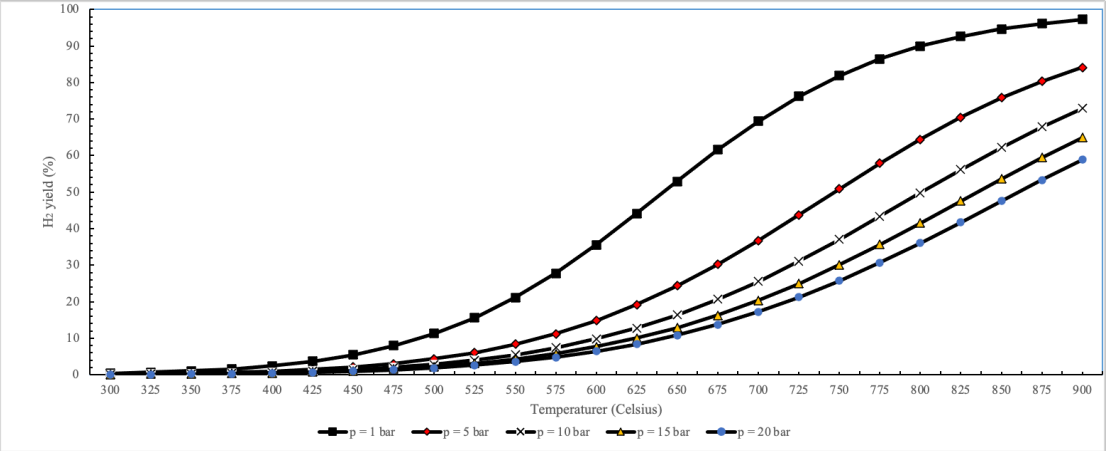

Figure 2: Temperature and pressure effect on the H_2 yield.

3.1.2. Effect of CH_4 to CO_2 ratio

In Figure 3 the H_2 yields and the molar flow rates of H_2 flowing out of the reactor are plotted at varying CH_4/CO_2 ratios. It was found that the maximum yield and flow rate decreased as the CH_4/CO_2 ratio increased for a constant feed rate of 1 kmol/h. Identical trends were observed for the CH_4 and CO_2 conversion, the CO yield, and the duty. Their corresponding figures can be found in Appendix A-5, A-6, A-7, and A-8 respectively.

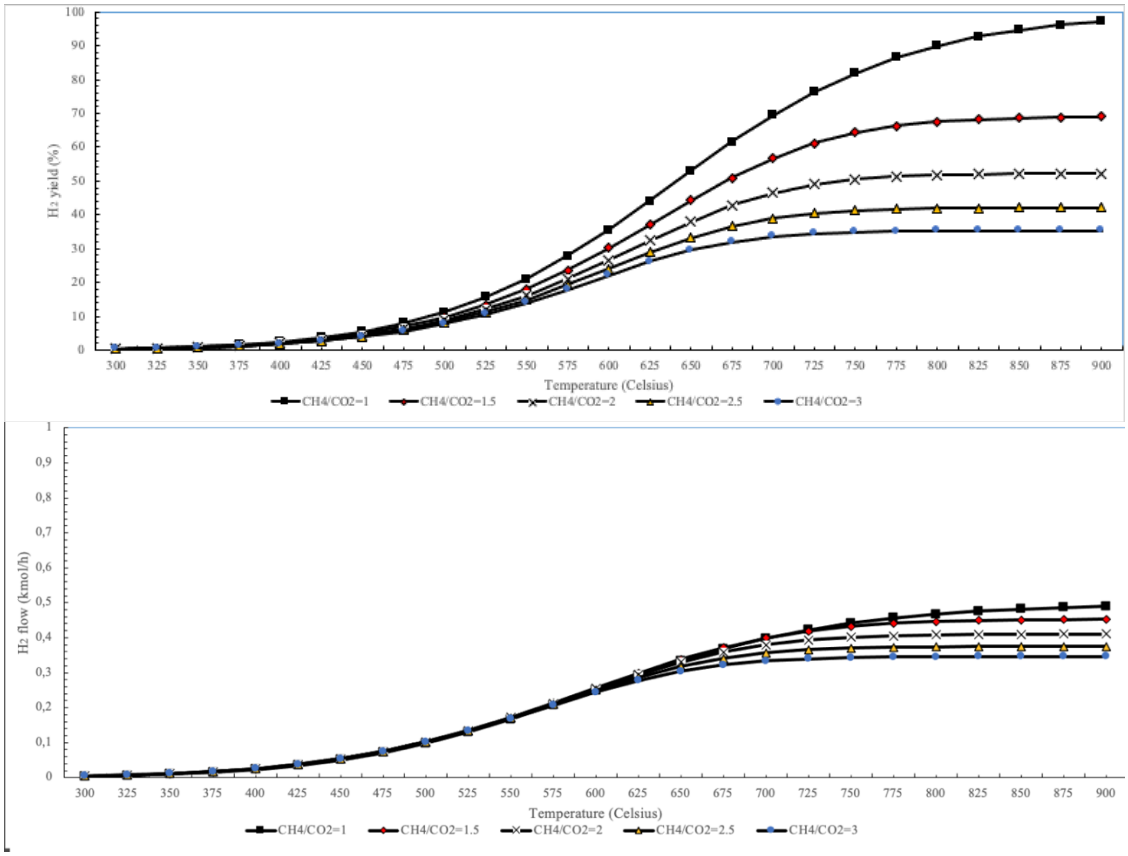

Figure 3: Effect of the CH_4/CO_2 ratio on A) the H_2 yield B) the molar flow rate of H_2

3.1.3. Effect of H2O in the feed

Figure 4 displays the H_2 yield at different temperatures for different molar fractions of H2O in the feed. The presence of H_2O in the feed positively affects the H_2 yield at temperatures below 650-750°C. The temperature corresponding to the maximum yield depends on the molar fraction of H_2O in the feed, requiring a higher temperature with lower amounts of H_2O in the feed. The increase in yield is caused by the MSR and WGS reactions and becomes more pronounced with more H_2O in the feed (60%). At higher temperatures, the RWGS reaction becomes more prevalent. This leads to a clear decrease in H_2 yield at temperatures higher than 700°C when the feed consists of 60% H_2O. Figure 5 displays the CO_2 conversion at different temperatures for varying amounts of H_2O in the feed. A similar result was found where the CO_2 conversion is negative at lower temperatures because of the WGS reaction. The effect is inversed compared to the H_2 yield, as CO_2 is produced alongside H_2. It is visible at higher temperatures that as the H_2 yield decreases, the CO_2 conversion increases, as H_2 and CO_2 react into H_2O and CO. The CH_4 conversion, CO yield, and duty display similar patterns as in section 3.1.1.

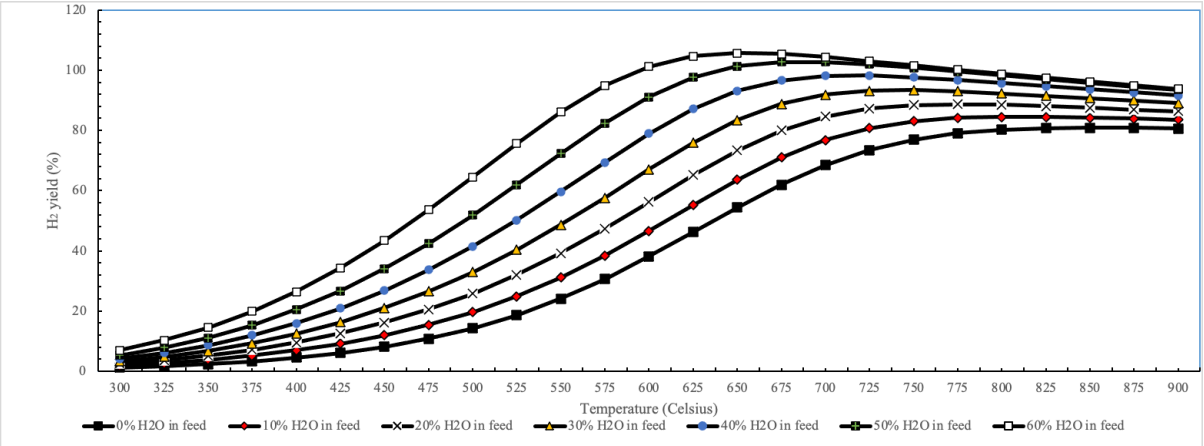

Figure 4: Effect of the presence of H_2O in the feed on the H_2 yield

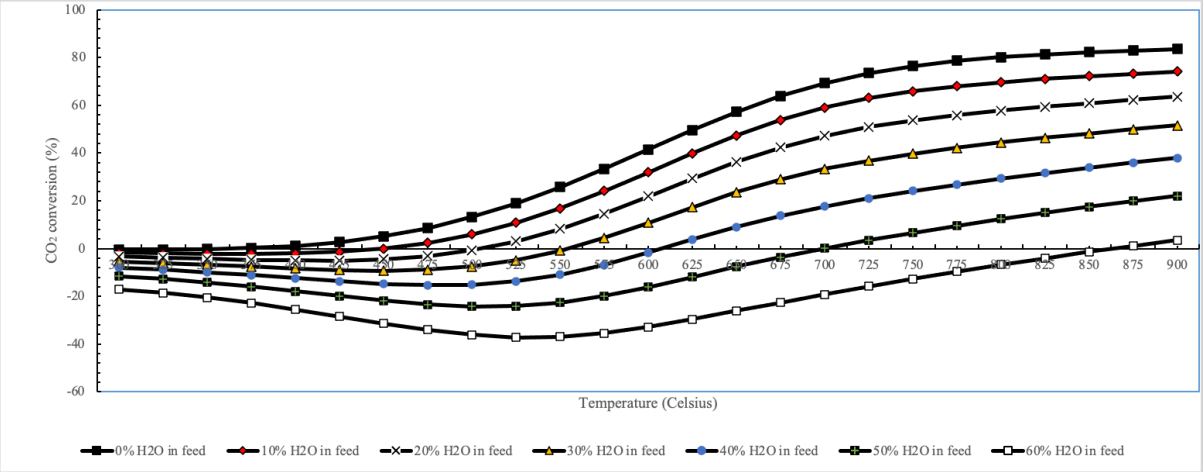

Figure 5: Effect of the presence of H_2O in the feed on the CO_2 conversion

3.2. Membrane model

3.2.1. Selecting the number of sub-reformers (n)

Figure 6 shows a comparison of the H_2 yield obtained from membrane models using different values for n. The H_2 yield was plotted on the y-axis against the temperature. For low values of n, the H_2 is heavily dependent on the temperature. This dependency decreases as the value of n increases, as can be seen for the case where $n = 50$. Additionally, at higher temperatures, the obtained H_2 yields start to converge at higher temperatures. The value of n was chosen to be 50, as it achieved the highest yields at low temperatures.

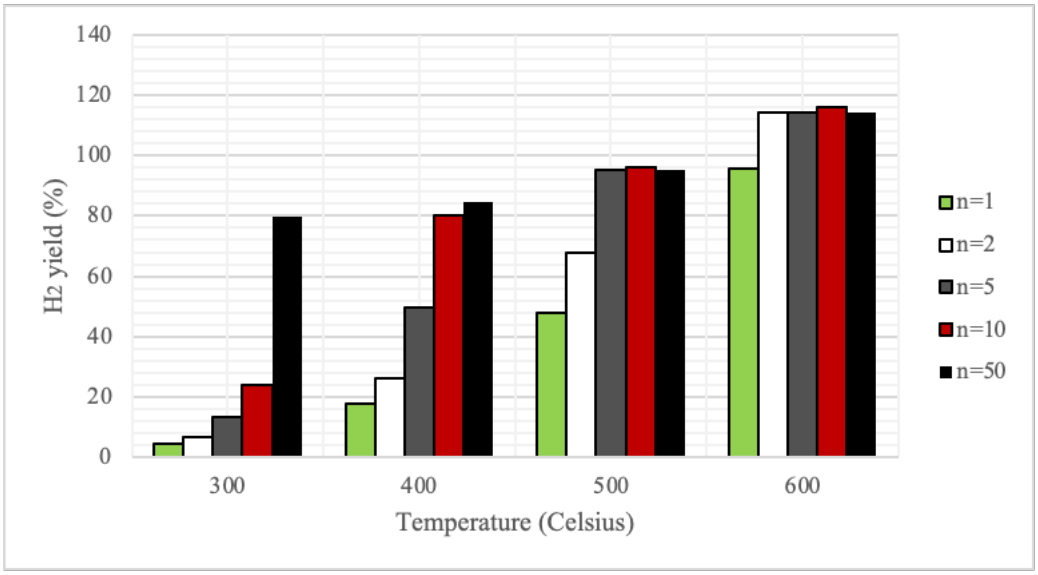

Figure 6: H2 yields using n number of sub-reformers at varying temperatures

Figure 6A shows that the H_2 yield can be considered independent of n, due to the low permeation capacity of the membrane. In Figure 6B, the effect of changing n becomes much more significant, especially at lower temperatures. In the case of $n = 50$, the H_2 yield is 80% at 300°C, whereas a temperature close to 600°C is required to reach the same yield when $n = 1$. At higher temperatures, the differences between the cases of n become less pronounced, as the reactions are less restricted by the thermodynamic equilibrium of the reactions.

In addition, for the cases where n had the values of 1, 2, 5, and 10, warnings were reported by Aspen Plus for the sub-separators. This likely happened since the amount of H_2 that was removed from the retentate stream was less than the given input of the sub-separators. This suggests that the extent of the reaction is the limiting factor, instead of the membrane permeation capacity. Furthermore, this aligns with the results in Figure 6A, where n does not have a significant effect on the H_2 yield. Thus, to make a comparison between the membrane model and the base case model, the results were used for the case in which $n = 50$.

3.2.2. Comparison of the H_2 yields obtained from the base and the membrane model

Figure 7 provides a comparison of the H_2 yield between the base case model and the membrane model at increasing pressures. Figure 7A shows that the H_2 yield is similar for both models at a pressure of 2 bar in the reactor. In Figure 7B, the differences in yield become more noticeable. At 300°C a H_2 yield close to 40% is obtained from the membrane model, whereas a yield of 6% is achieved for the base case model. As the temperature increases, the results of each model start to converge. Figure 7C shows the results for each model at a reactor pressure of 11 bar.

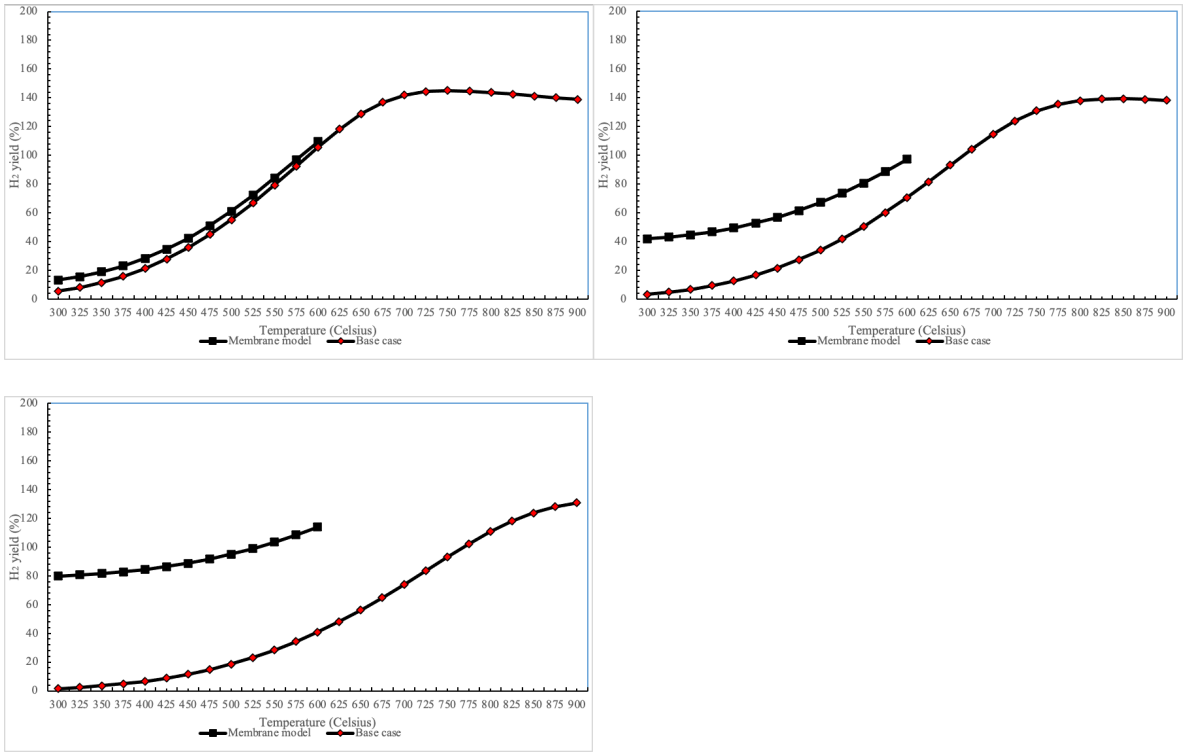

Figure 7: Comparison of the H_2 yield between the membrane model and the base case model at different pressures A) 2 bar B) 6 bar C) 11 bar

For the base case model was found that the maximum yield decreases when the system is pressurised. In addition, a higher temperature is required to attain the maximum H_2 yield. In the case of the membrane model, the maximum attainable yield was outside of the temperature range that was used to model the system, as the yield has not started decreasing. Thus, the maximum H_2 yield for the membrane model was taken as the yield at 600°C. In addition, the maximum yield increased when changing the pressure from 6 bar to 11 bar, as the membrane capacity increased, overcoming yield loss due to an increase in pressure.

In each case, the base model achieved the highest H_2 yield. The membrane model outperforms the base case model under identical operating conditions, especially under higher pressures. However, it is currently held back by the temperature and pressure resistance of the membrane. The base case model can be run at much higher temperatures, which allows it to achieve higher yields.

3.2.3. Comparison of the CO yield obtained from the base and the membrane model

The CO yields obtained from the simulations of each model. Figure 8A and 8B show that at lower temperatures, the CO yield is higher for the membrane model, as more H_2 is produced through the MDR and MSR reactions. The CO yield for the base case model starts to increase steadily as the RWGS reaction becomes more prevalent.

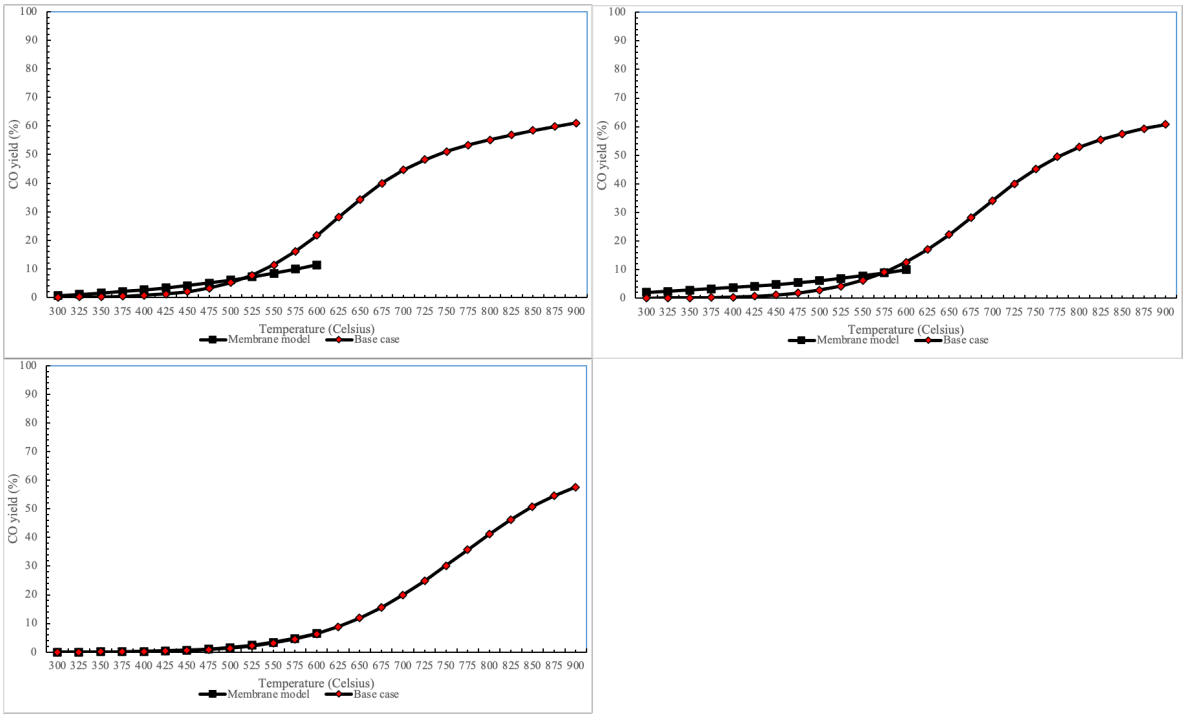

Figure 8: Comparison of the CO yield between the membrane model and the base case model at different pressures A) 2 bar B) 6 bar C) 11 bar

The temperature range at which the membrane model was ran was not wide enough to study the full effect of the RWGS reaction on the membrane model. However, an intersection can be found between the results of each model in Figure 8A and 8B. This indicates that base case model is more affected by the RWGS reaction than the membrane model. The CO yield for the membrane model seems to increase linearly, even after the RWGS reaction has become more prominent in the base case model, suggesting it is not affecting the membrane model at the temperature range at which the model was run. The CO yield decrease for both models when moving from Figure 8A to Figure 8C.

3.2.4. Comparison of the CO_2 conversion from the base and the membrane model

As explained in section 2.1, CO_2 is formed during the WGS reaction. As a result, the CO_2 conversion may become negative. This effect is visible for both models in each graph in Figure 9. For the base case model, the WGS reaction is most prevalent at temperatures around 550-650°C, which is at the lowest CO_2 conversion. At temperatures above the minimum conversion temperature, the CO_2 conversions for the base case model follow similar trends as the CO yield in Figure 8, indicating that CO is produced from CO_2 through the RWGS reaction. As the CO_2 conversion increases, the H_2 starts to decline when the feed contains enough H_2O. Additionally, the minimum of the graph moves towards the x-axis as the pressure is increased.

Figure 8A shows that the membrane model produces similar amounts of CO_2 under these operating conditions as the base model. In 8B, the differences are more pronounced. In 8C, the CO_2 conversion decreases from around -35% to around -80% at lower temperatures. As a result, the produced H_2 does not exhaust GHGs when burned, but CO_2 is released during its production.

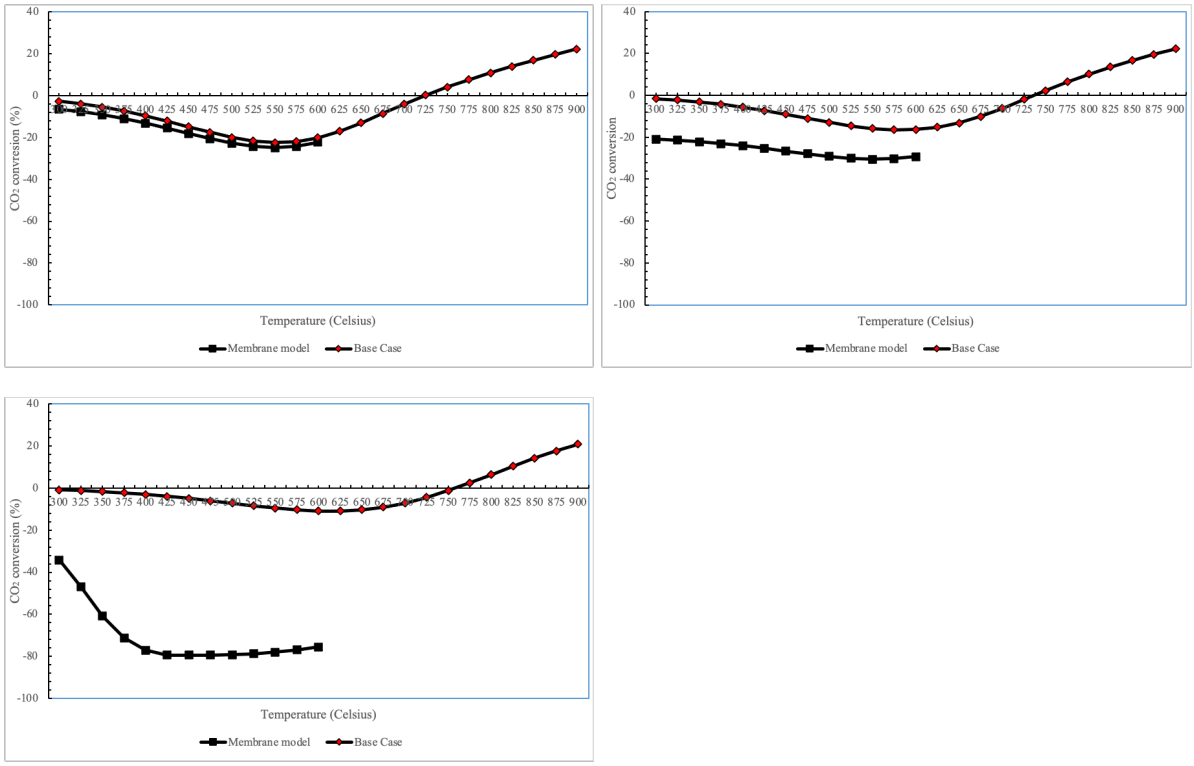

Figure 9: Comparison of the CO_2 conversion between the membrane model and the base case model at different pressures A) 2 bar B) 6 bar C) 11 bar

3.2.5. Comparison of the CH_4 conversion from the base and the membrane model

Like Figures 7, 8, and 9, the results for both models are similar when the system is run at 2 bar pressure. In Figures 10A and 10B, the membrane model outperforms the base case model at the same temperature, but the results start to converge as the temperature increases. The base case model can achieve a 100% CH_4 conversion in Figures 10A and 10B. The maximum CH_4 conversion is shifted towards the right and decreases as the pressure is increased.

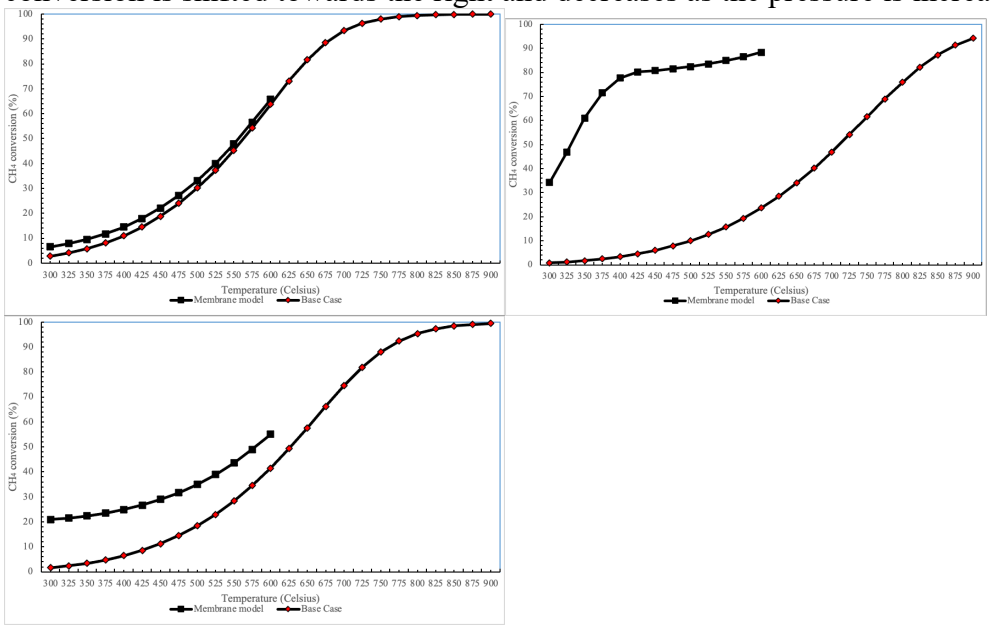

Figure 10: Comparison of the CH_4 conversion between the membrane model and the base case model at different pressures A) 2 bar B) 6 bar C) 11 bar

In Figure 10C, considerable CH_4 conversions are attained at relatively low temperatures. It follows a similar trend as the results for the membrane model in Figure 9C, where the slope of the graph decreases around 425°C.

3.2.5. Comparison of the reactor duty from the base and the membrane model

Figure 11 plots the H_2 yield against the duty required to achieve the yield for each model. The bottom x-axis shows the duty for the membrane model, the top x-axis shows the duty for the base case model using a feed flow rate of 1 kmol/h.

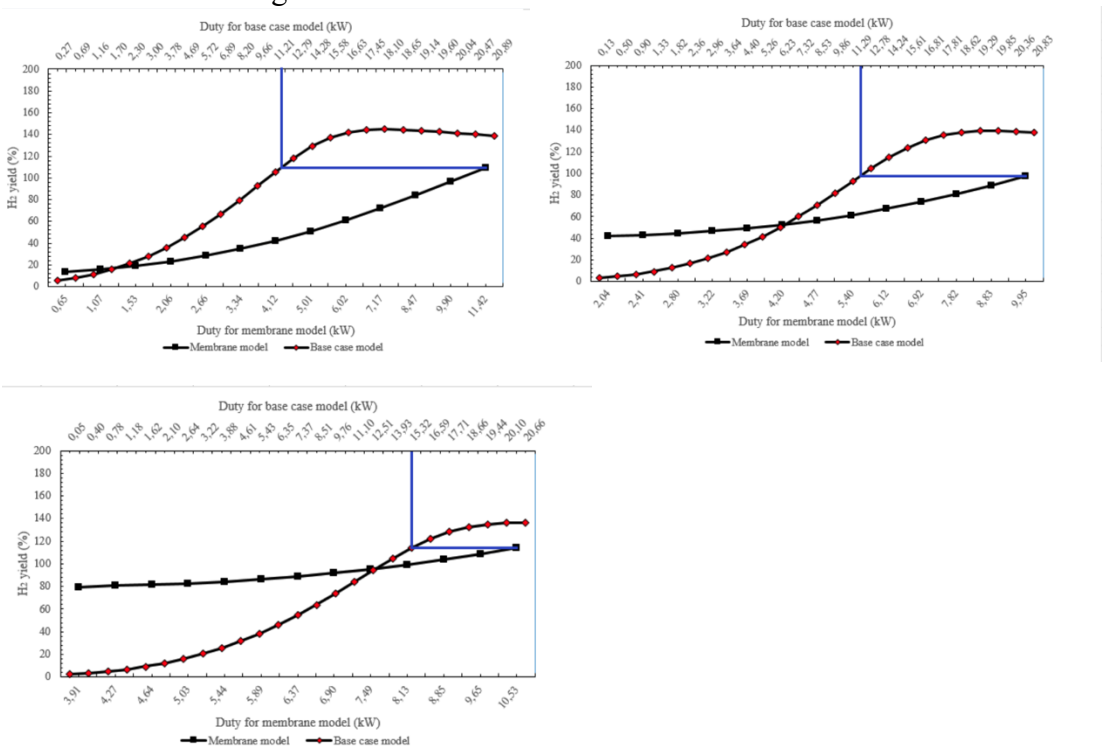

Figure 11: Comparison of the reactor duty between the membrane model and the base case model at different pressures A) 2 bar B) 6 bar C) 11 bar

A horizontal line was drawn from the highest H_2 achieved by the membrane model to the same yield achieved by the base model to find the corresponding duty. At a pressure of 2 bar was found that the duty for the membrane model was slightly higher, 11.42 kW compared to approximately 11.21 kW. At higher pressures, the membrane model used a lower duty than the base model, 9.95 compared to approximately 11.29 kW at 6 bar and 10.53 kW compared to approximately 15.3 kW at 11 bar.

4. Conclusion

The optimal operating conditions were found for a bi-reforming system without a membrane. From the range of the variables that were tested, it was found that the system performed the best at a high operating temperature, atmospheric pressure, using a molar fraction of 0.60 for H_2O in the feed, and using a CH_4/CO_2 of 1.

Despite the increase in performance of the membrane model when increasing the pressure, the membrane model does not achieve higher yields and conversions than the base model. The base model achieved the highest H_2 and CO yields, and CH_4 and CO_2 conversions, because it

was able to run at higher temperatures. However, under the same reaction temperature, the membrane model performed better than the base model.

Membranes are currently held back by factors such as operating temperature and pressure, permeability, and poisoning. The use of an electrochemical membrane might offer a solution, as it does not use pressure as a driving force and can run at higher temperatures. This allows the system at higher temperatures and retain a high separation factor while operating at atmospheric pressure, thereby not compromising the system performance.

Currently, bi-reforming systems without membranes can achieve higher performance than bi-reforming systems using membrane reactors. However, the membrane systems result in a lower duty, making it a more sustainable process.

References

Minh, D. P., Siang, T. J., Vo, D. V. N., Phan, T. S., Ridart, C., Nzihou, A., & Grouset, D. (2018). Hydrogen production from biogas reforming: An overview of steam reforming, dry reforming, dual reforming, and tri-reforming of methane. In *Hydrogen Supply Chain: Design, Deployment and Operation* (pp. 111–166). Elsevier. https://doi.org/10.1016/B978-0-12-811197-0.00004-X

Rostrup-Nielsen, J. R. (2000). New aspects of syngas production and use. *Catalysis Today*, *63*(2–4), 159–164.

Dry, M. E. (2002). The Fischer-Tropsch process: 1950-2000. In *Catalysis Today* (Vol. 71).

Balagurusamy, N. (2021). *Biogas Production: From Anaerobic Digestion to a Sustainable Bioenergy Industry* (A. Chandel, Ed.). Springer Publishing.

Parente, M., Soria, M. A., & Madeira, L. M. (2020). Hydrogen and/or syngas production through combined dry and steam reforming of biogas in a membrane reactor: A thermodynamic study. *Renewable Energy*, *157*, 1254–1264. https://doi.org/10.1016/j.renene.2020.05.023

Scheutz, C., Kjeldsen, P., & Gentil, E. (2009). Greenhouse gases, radiative forcing, global warming potential and waste management - An introduction. In *Waste Management and Research* (Vol. 27, Issue 8, pp. 716–723. https://doi.org/10.1177/0734242X09345599

Ruiz, D., San Miguel, G., Corona, B., Gaitero, A., & Domínguez, A. (2018). Environmental and economic analysis of power generation in a thermophilic biogas plant. *Science of the Total Environment*, *633*, 1418–1428. https://doi.org/10.1016/j.scitotenv.2018.03.169

Scarlat, N., Dallemand, J. F., & Fahl, F. (2018). Biogas: Developments and perspectives in Europe. In *Renewable Energy* (Vol. 129, pp. 457–472). Elsevier Ltd. https://doi.org/10.1016/j.renene.2018.03.006

Sarker, B. R., Wu, B., & Paudel, K. P. (2018). Optimal number and location of storage hubs and biogas production reactors in farmlands with allocation of multiple feedstocks. *Applied Mathematical Modelling*, *55*, 447–465. https://doi.org/10.1016/j.apm.2017.11.010

Zhao, X., Joseph, B., Kuhn, J., & Ozcan, S. (2020). *iScience Review Biogas Reforming to Syngas: A Review*. https://doi.org/10.1016/j.isci

Rasi, S., Veijanen, A., & Rintala, J. (2007). Trace compounds of biogas from different biogas production plants. *Energy*, *32*(8), 1375–1380. https://doi.org/10.1016/j.energy.2006.10.018

Gao, Y., Jiang, J., Meng, Y., Yan, F., & Aihemaiti, A. (2018). A review of recent developments in hydrogen production via biogas dry reforming. In *Energy Conversion and Management* (Vol. 171, pp. 133–155). Elsevier Ltd. https://doi.org/10.1016/j.enconman.2018.05.083

Wang, Y., Yao, L., Wang, S., Mao, D., & Hu, C. (2018). Low-temperature catalytic CO2 dry reforming of methane on Ni-based catalysts: A review. In *Fuel Processing Technology* (Vol. 169, pp. 199–206). Elsevier B.V. https://doi.org/10.1016/j.fuproc.2017.10.007

Matsumura, Y., & Nakamori, T. (2004). Steam reforming of methane over nickel catalysts at low reaction temperature. *Applied Catalysis A: General*, *258*(1), 107–114. https://doi.org/10.1016/j.apcata.2003.08.009

Kumar, N., Shojaee, M., & Spivey, J. J. (2015). Catalytic bi-reforming of methane: From greenhouse gases to syngas. In *Current Opinion in Chemical Engineering* (Vol. 9, pp. 8–15). Elsevier Ltd. https://doi.org/10.1016/j.coche.2015.07.003

Soria, M. A., Barros, D., & Madeira, L. M. (2019). Hydrogen production through steam reforming of bio-oils derived from biomass pyrolysis: Thermodynamic analysis including in situ CO2 and/or H2 separation. *Fuel*, *244*, 184–195. https://doi.org/10.1016/j.fuel.2019.01.156

Gallucci, F., Fernandez, E., Corengia, P., & van Sint Annaland, M. (2013). Recent advances on membranes and membrane reactors for hydrogen production. In *Chemical Engineering Science* (Vol. 92, pp. 40–66). Elsevier Ltd. https://doi.org/10.1016/j.ces.2013.01.008

Gallucci, F., Basile, A., & Ibney Hai, F. (2013). *Introduction - A review of membrane reactors*. In *A. Basile & F. Gallucci (Eds.),Membranes for membrane reactors: preparation, optimization and selection* (pp. 1-61). United Kingdom: John Wiley & sons. http://ro.uow.edu.au/eispapers/1153

Kluiters, S. C. A. (2004). *Status review on membrane systems for hydrogen separation*.

Kyriakou, V., Garagounis, I., Vourros, A., Vasileiou, E., Manerbino, A., Coors, W. G., & Stoukides, M. (2016). Methane steam reforming at low temperatures in a BaZr0.7Ce0.2Y0.1O2.9 proton conducting membrane reactor. *Applied Catalysis B: Environmental*, *186*, 1–9. https://doi.org/10.1016/j.apcatb.2015.12.039

Appendix

Section 3.1.1.

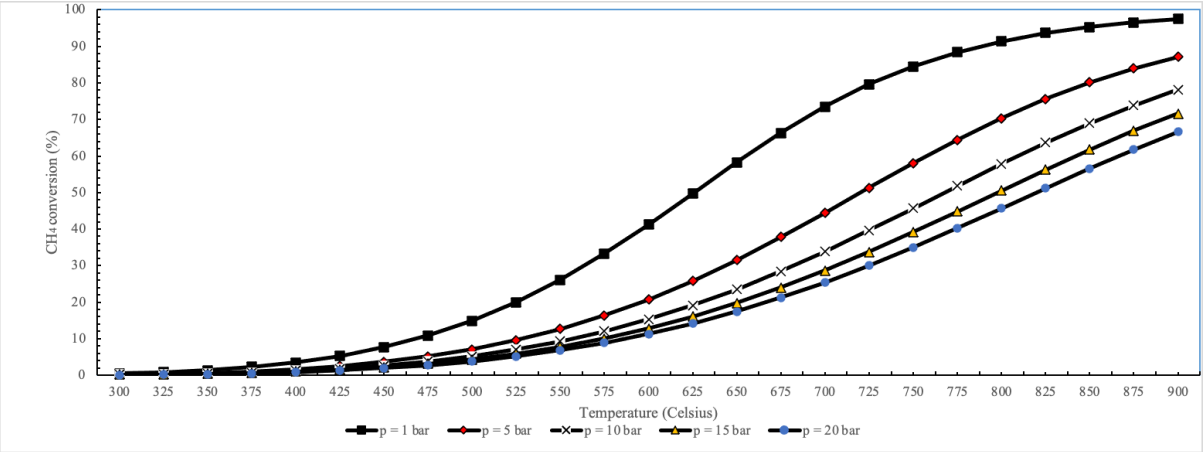

A - 1: The CH_4 conversion at varying temperatures and pressures

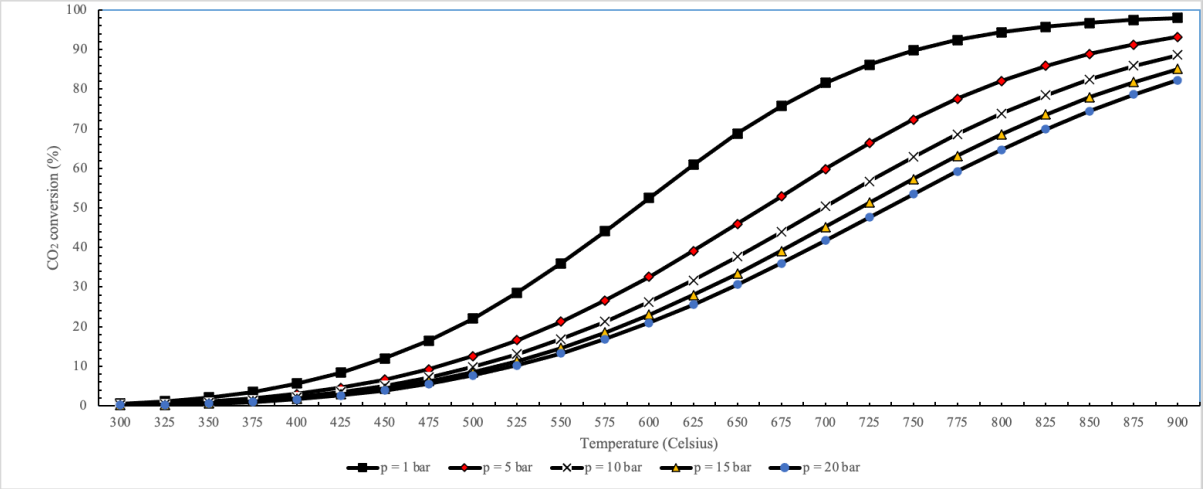

A - 2: The CO_2 conversion at varying temperatures and pressures

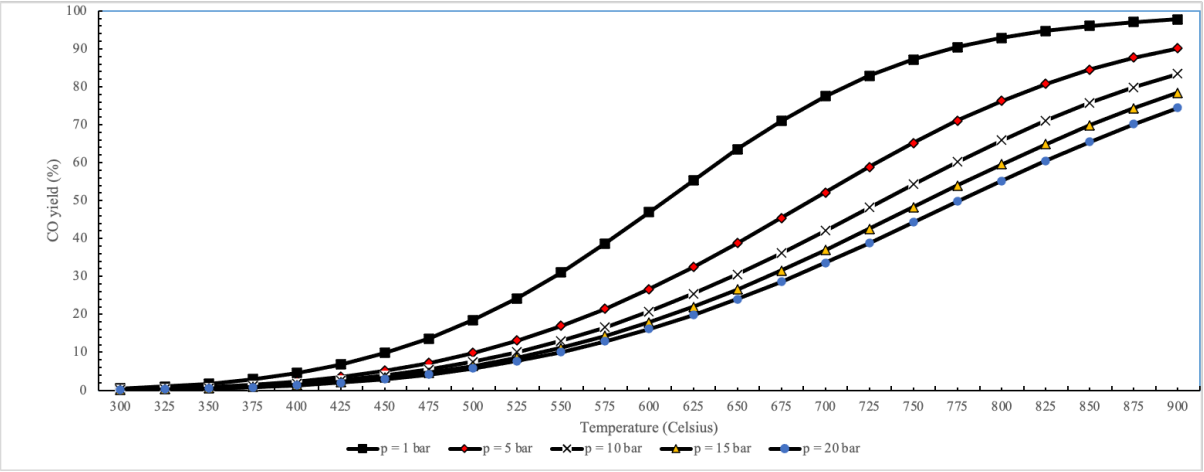

A - 3: The CO yield at varying temperatures and pressures

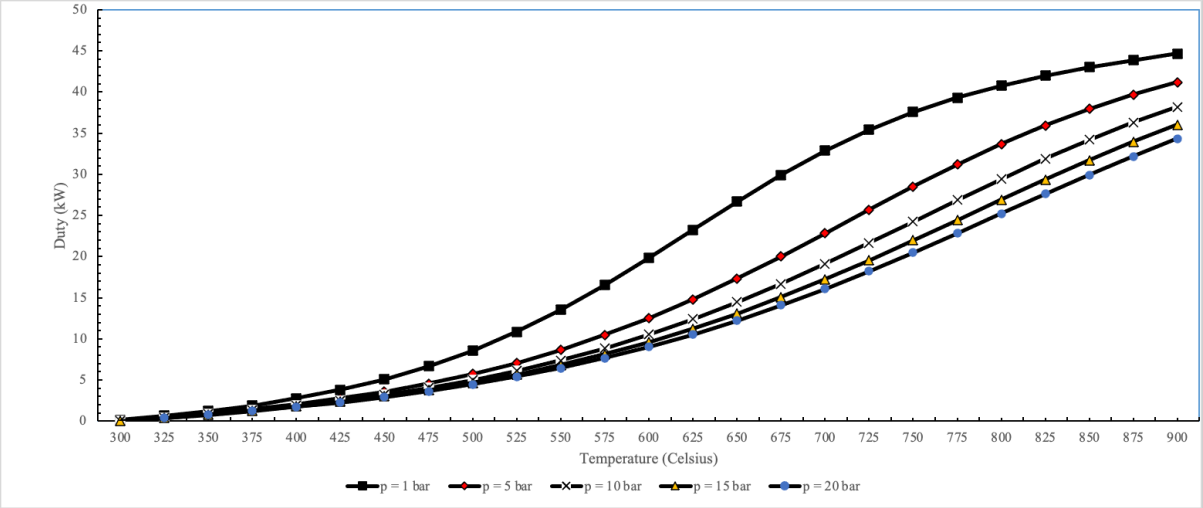

A - 4: The reactor duty at varying temperatures and pressures

Section 3.1.2.

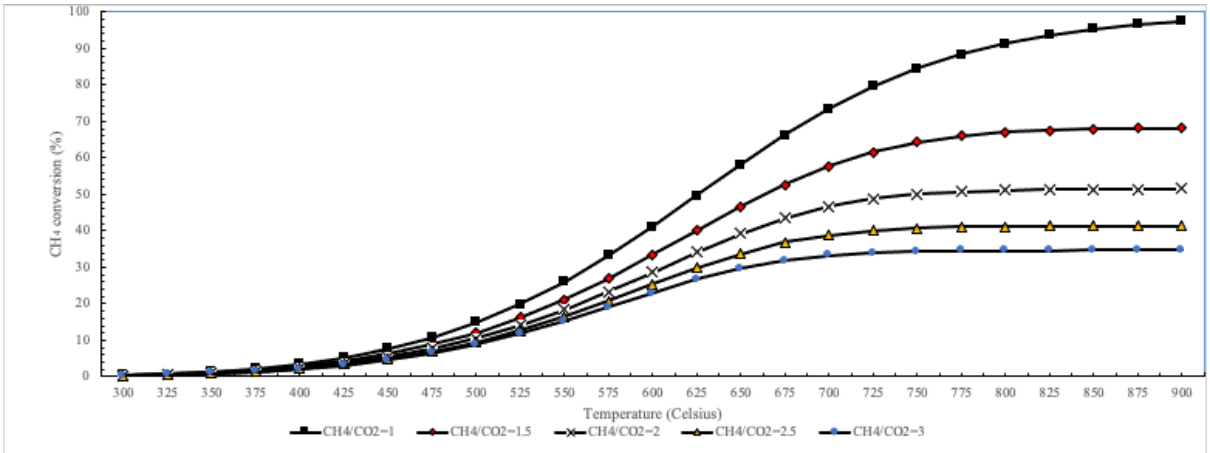

A - 5: The CH_4 conversion at varying temperatures and pressures

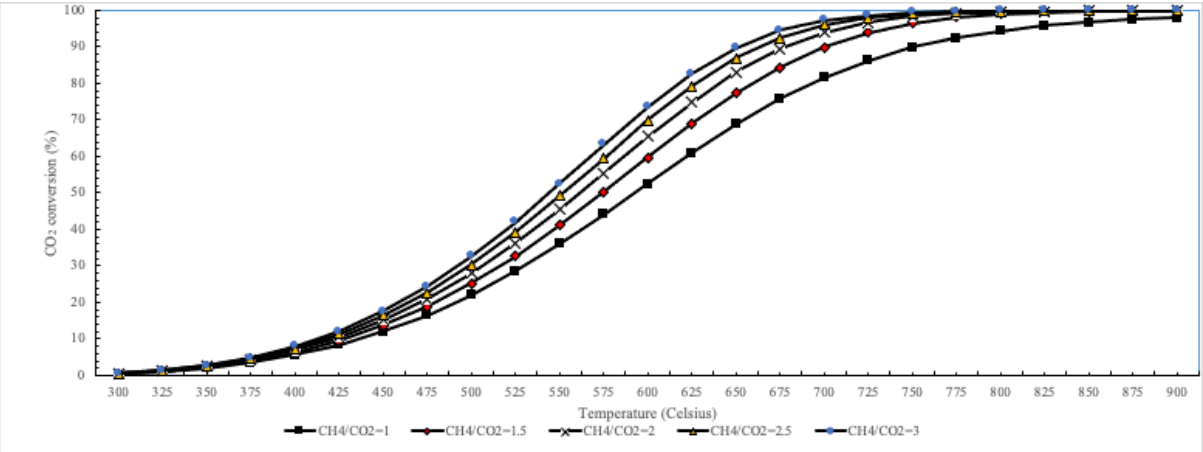

A - 6: The CO_2 conversion at varying temperatures and pressures

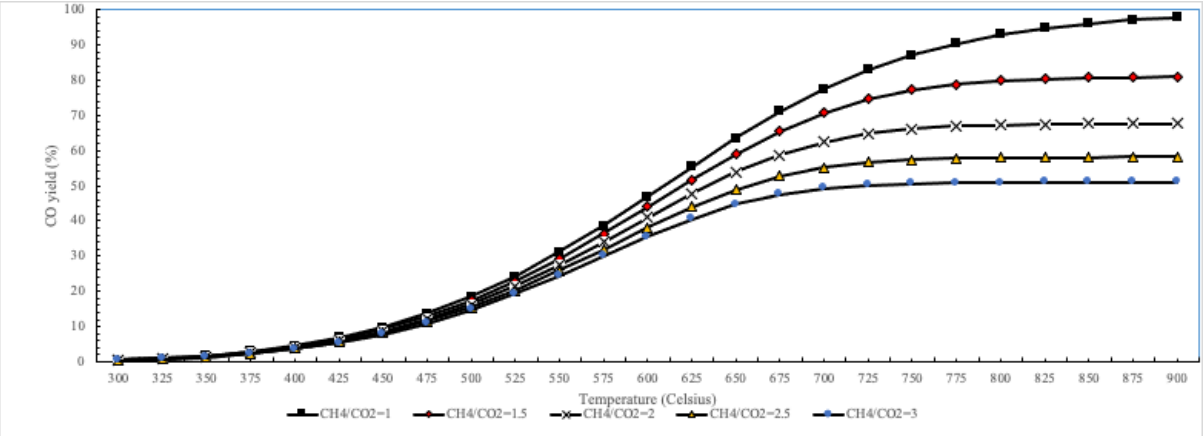

A - 7: The CO yield at varying temperatures and pressures

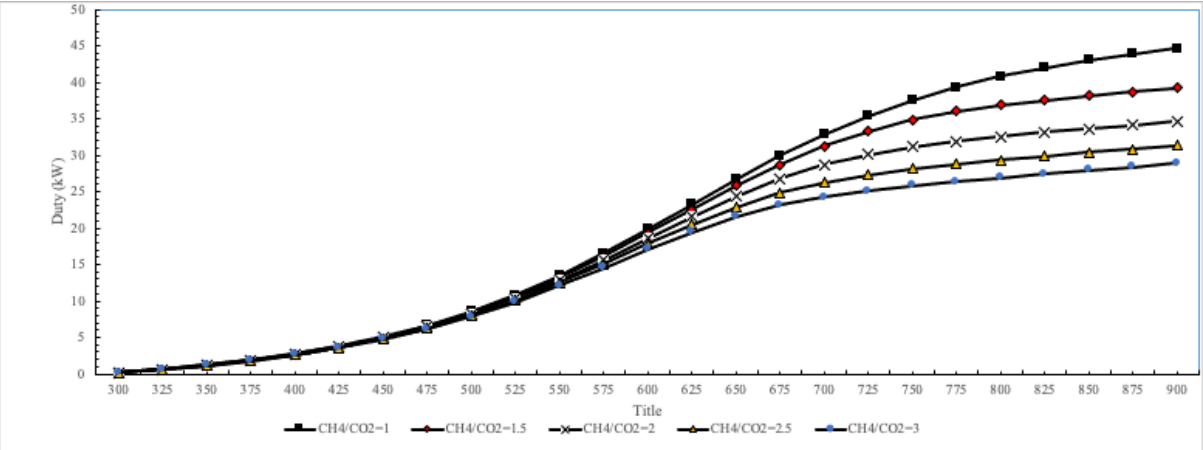

A - 8: The reactor duty at varying temperatures and pressures

Section 3.1.3.

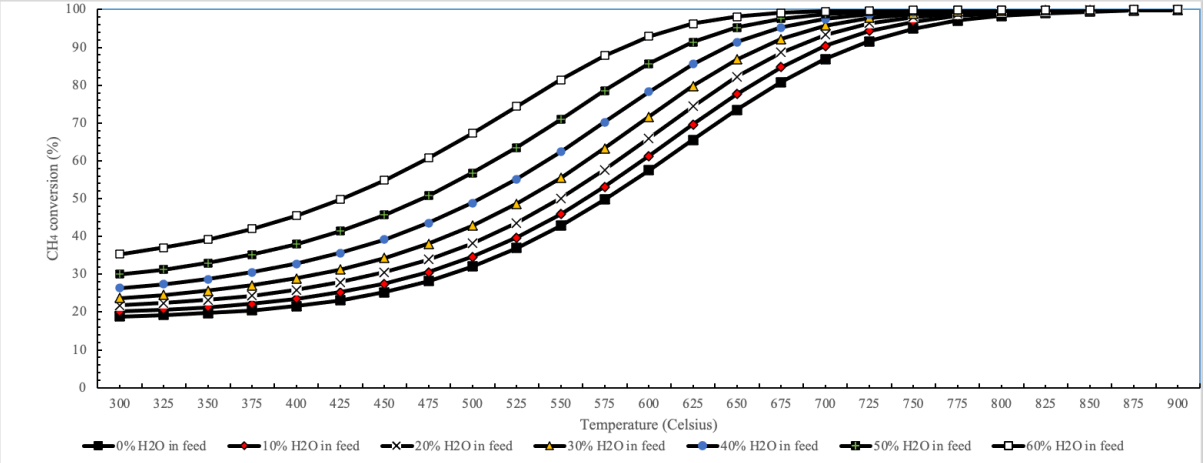

A - 9: The CH_4 conversion at varying temperatures and pressures

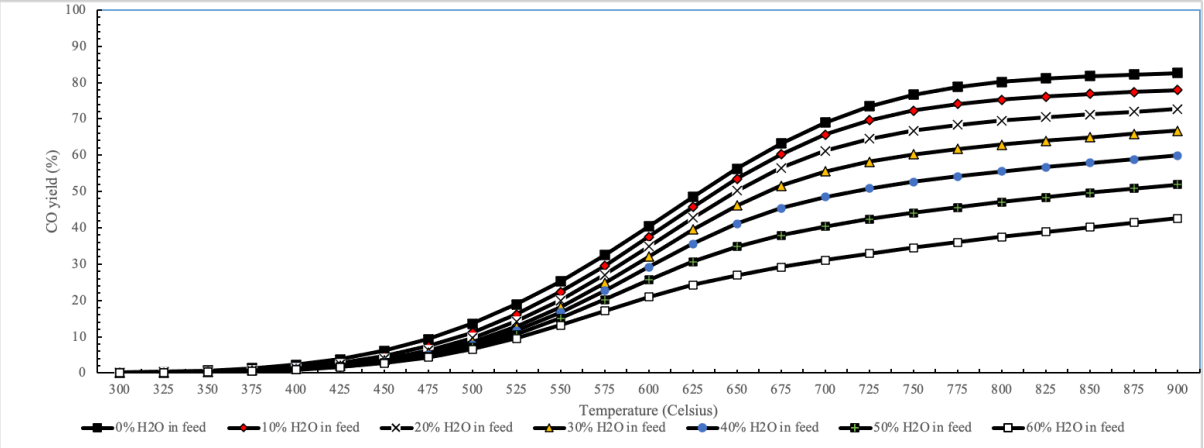

A - 10: The CO yield at varying temperatures and pressures

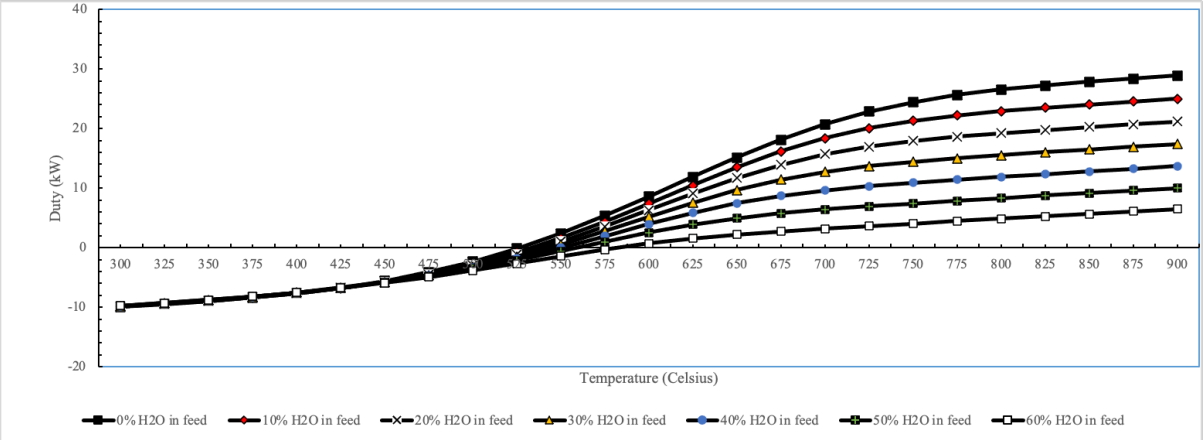

A - 11: The reactor duty at varying temperatures and pressures

Base case model for tri-reforming system

The effect of temperature and pressure

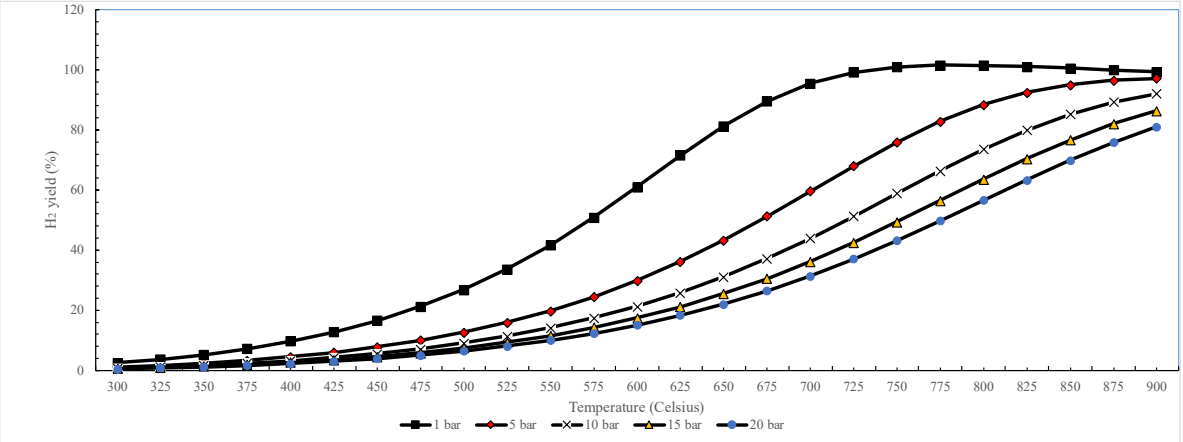

A - 12: The H_2 conversion at varying temperatures and pressures

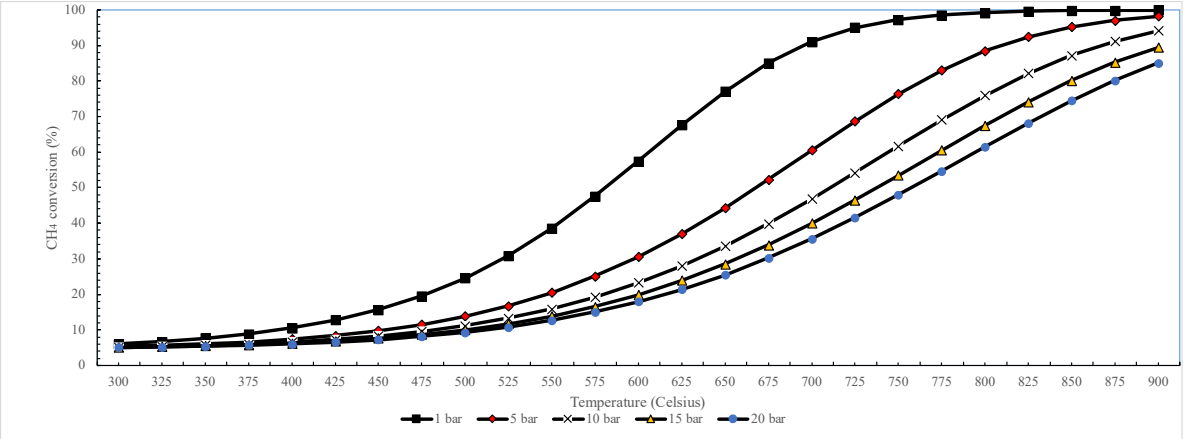

A - 13: The CH_4 conversion at varying temperatures and pressures

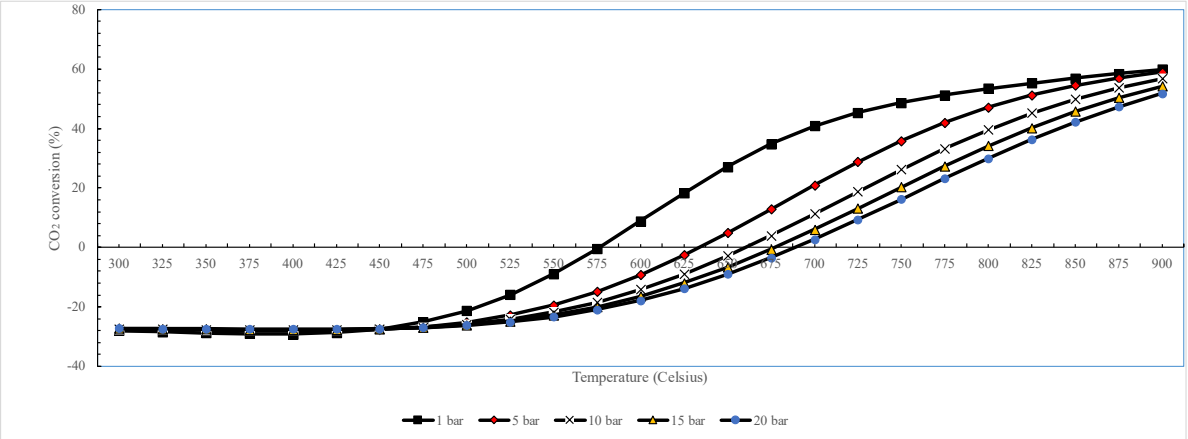

A - 14: The CO_2 conversion at varying temperatures and pressures

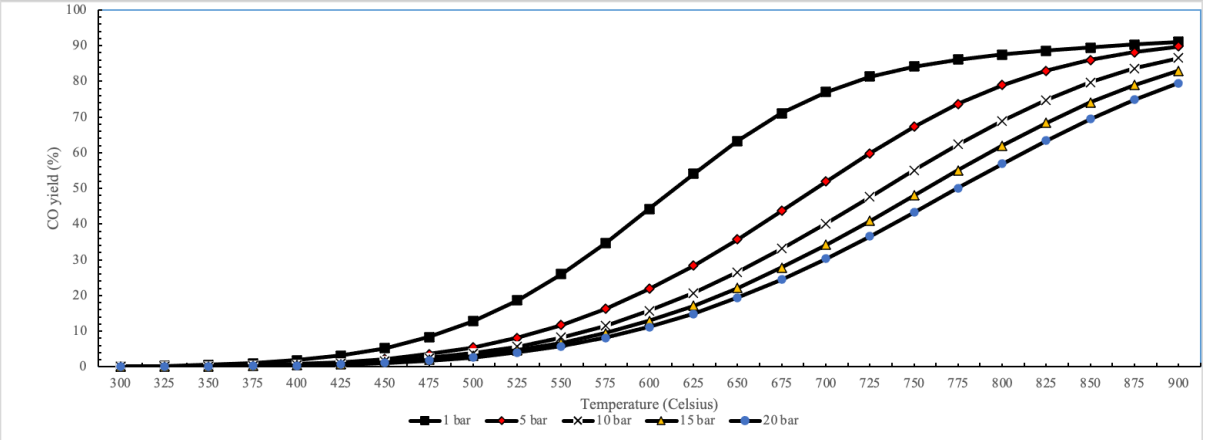

A - 15: The CO yield at varying temperatures and pressures

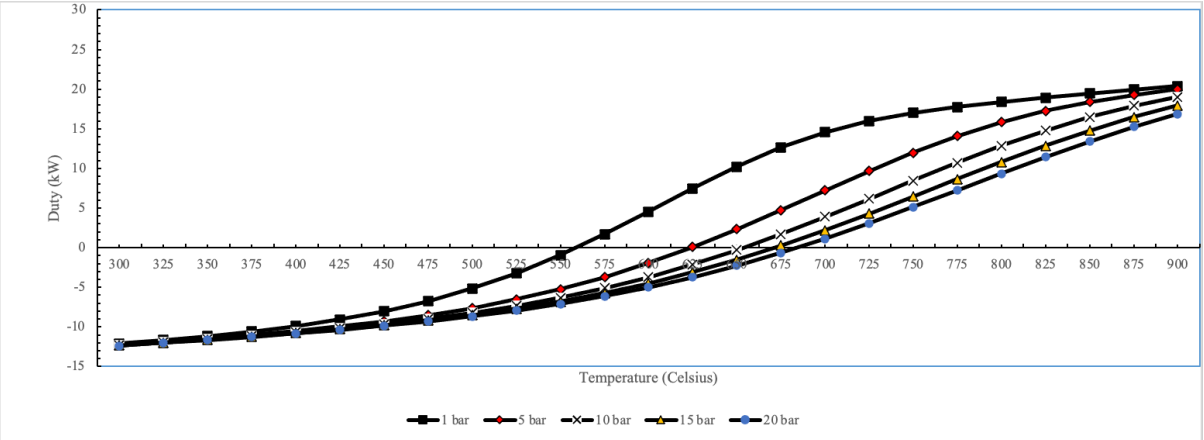

A - 16: The reactor duty at varying temperatures and pressures

Effect of varying amount of oxygen

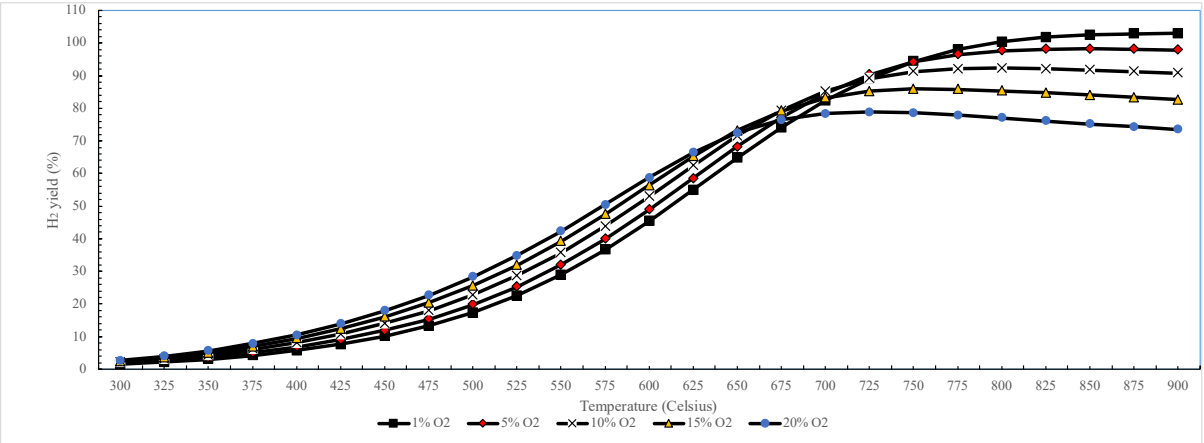

A - 17: The H_2 conversion at varying concentrations of O_2 in the feed

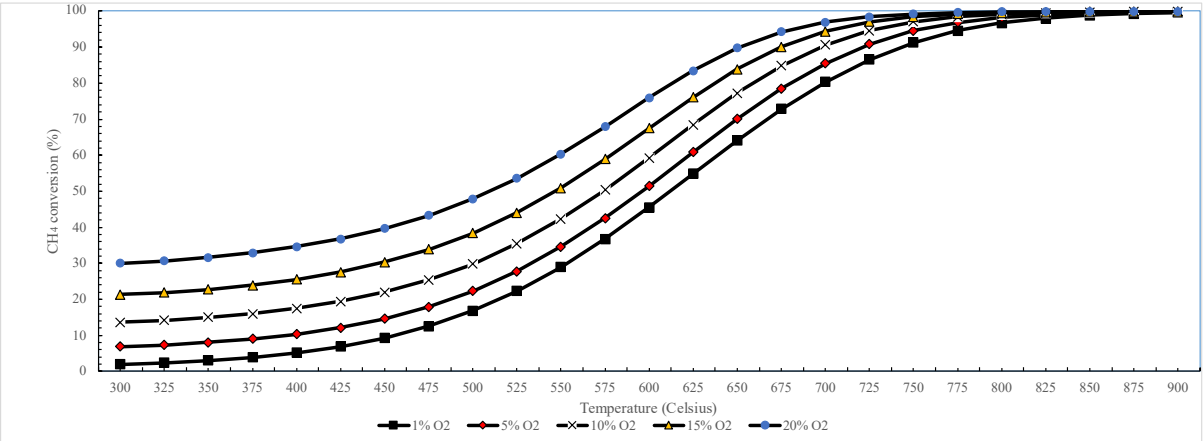

A - 18: The CH_4 conversion at varying concentrations of O_2 in the feed

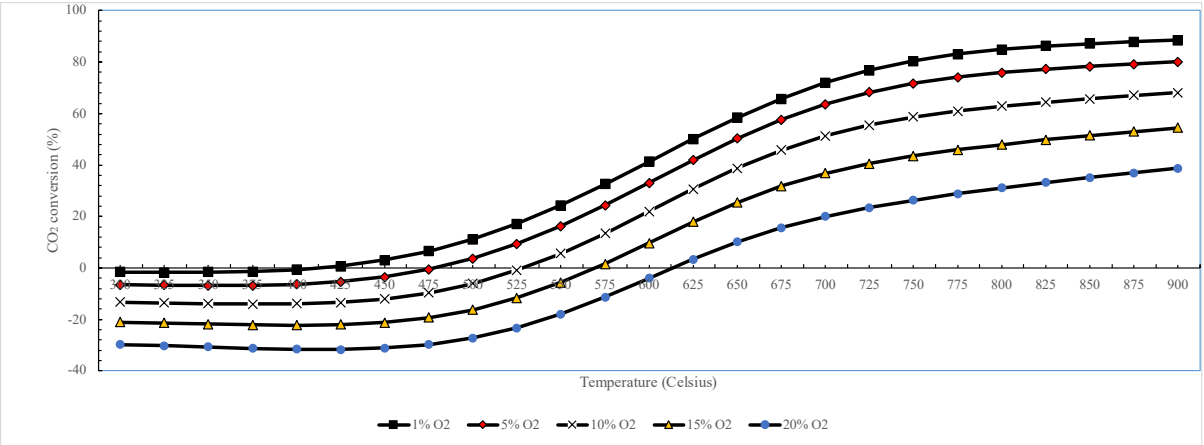

A - 19: The CO_2 conversion at varying concentrations of O_2 in the feed

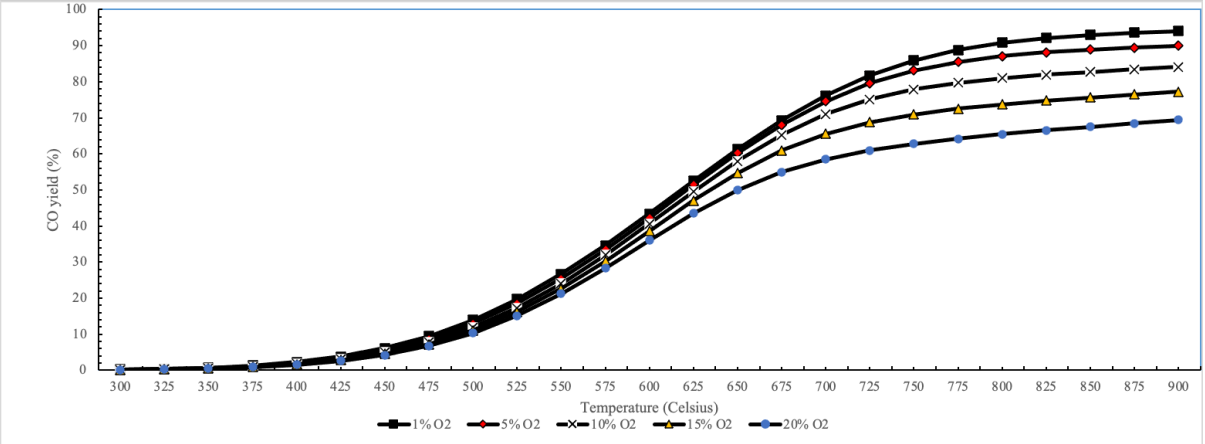

A - 20: The CO yield at varying concentrations of O_2 in the feed

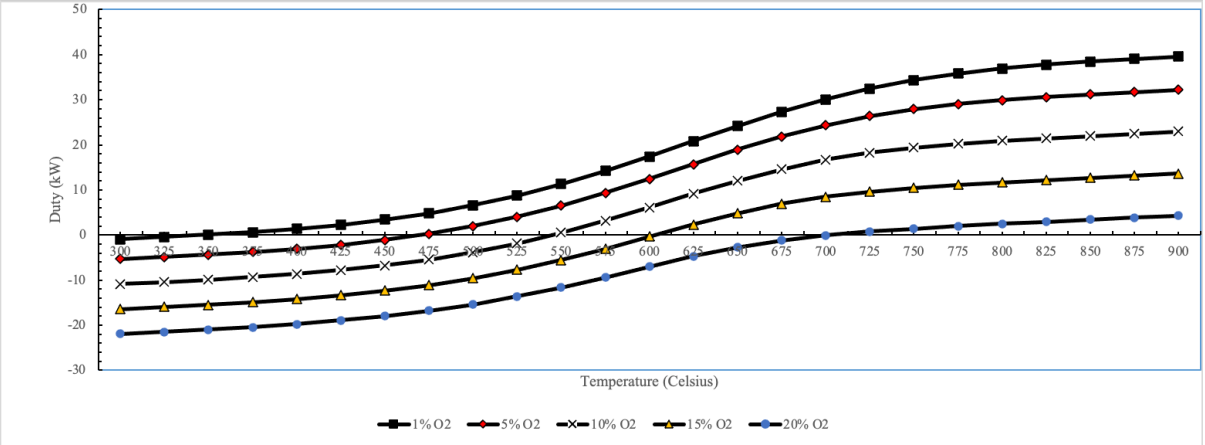

A - 21: The reactor duty at varying concentrations of O_2 in the feed

The effect of the CH_4/CO_2 ratio

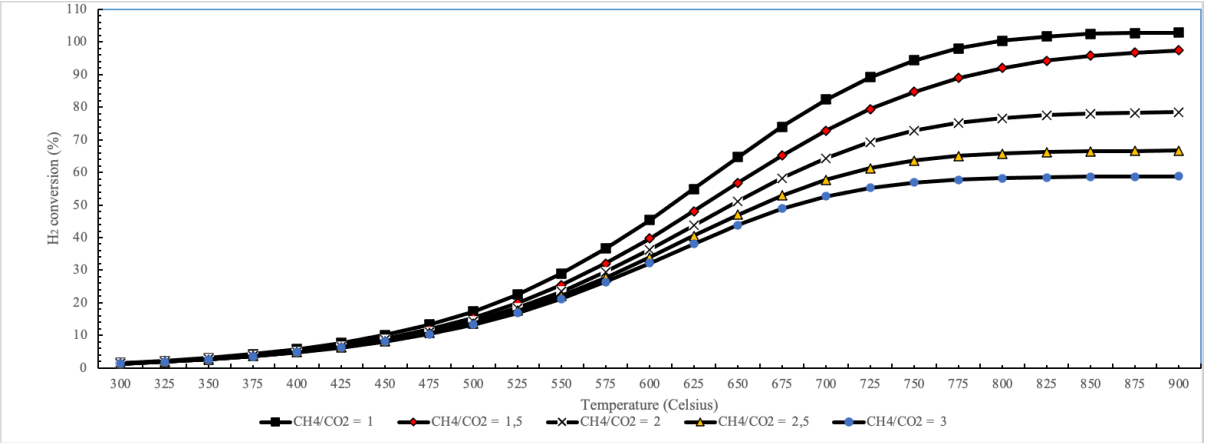

A - 22: The H_2 conversion at varying concentrations of CH_4/CO_2 ratios

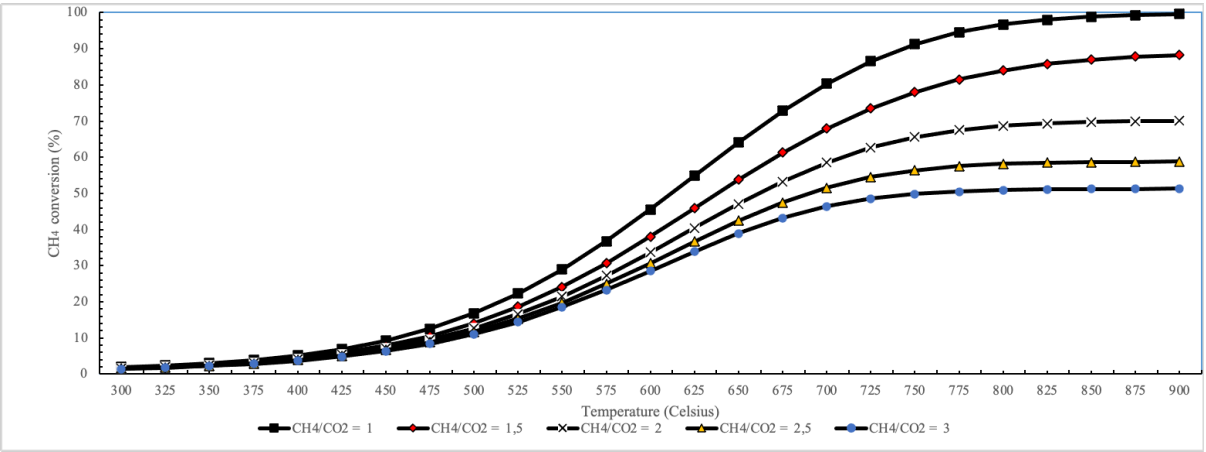

A - 23: The CH_4 conversion at varying concentrations of CH_4/CO_2 ratios

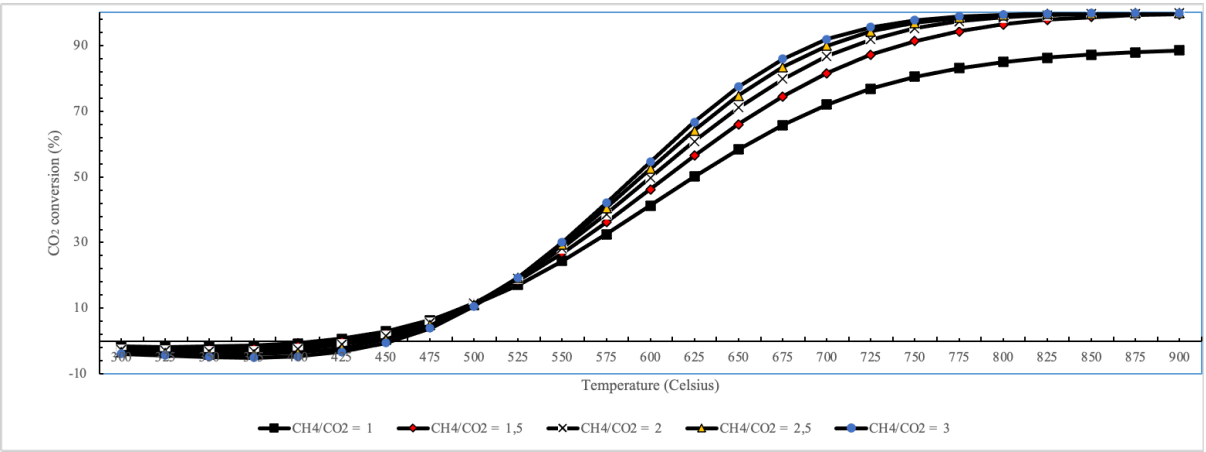

A - 24: The CO_2 conversion at varying concentrations of CH_4/CO_2 ratios

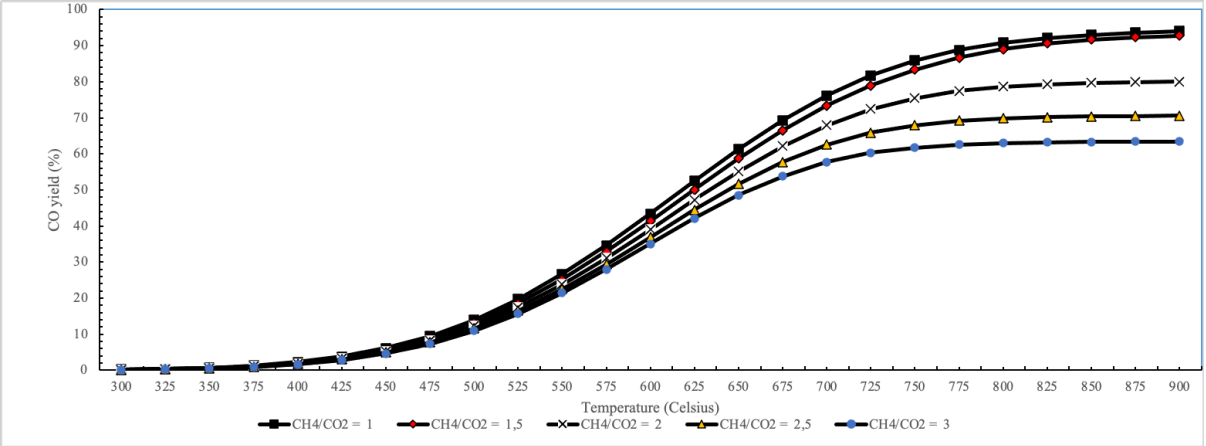

A - 25: The CO yield at varying concentrations of CH4/CO2 ratios

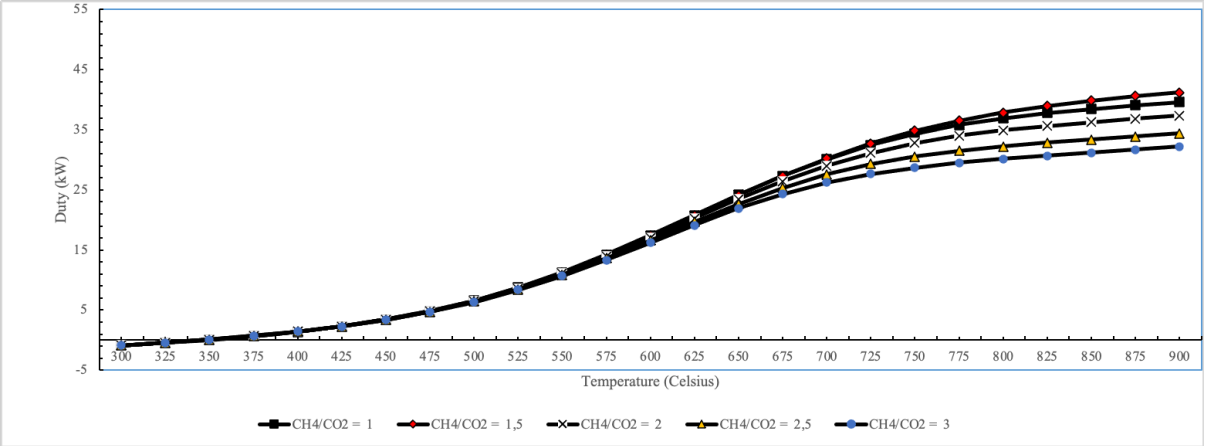

A - 26: The reactor duty at varying concentrations of CH4/CO2 ratios

Effect of varying amounts of H_2O in the feed

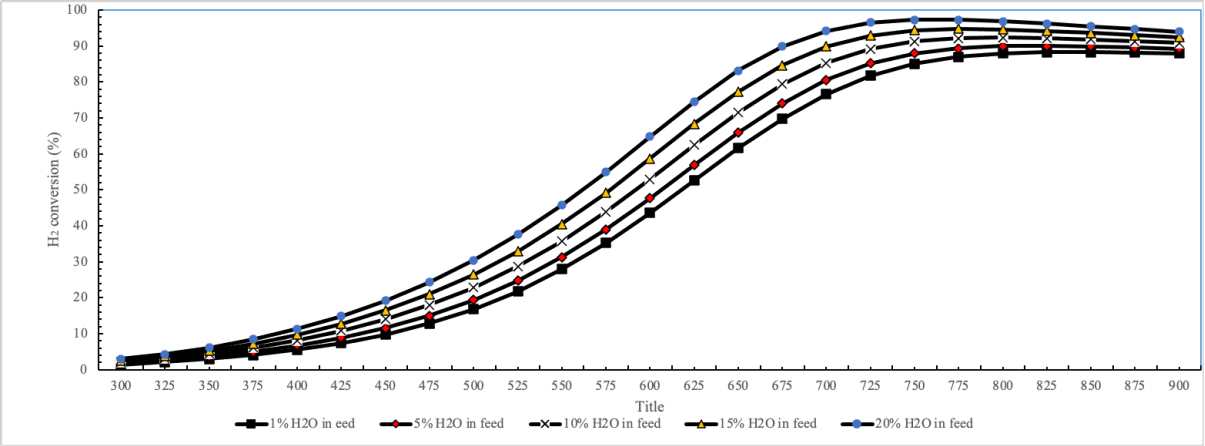

A - 27: The H_2 conversion at varying molar fractions of H_2O in the feed

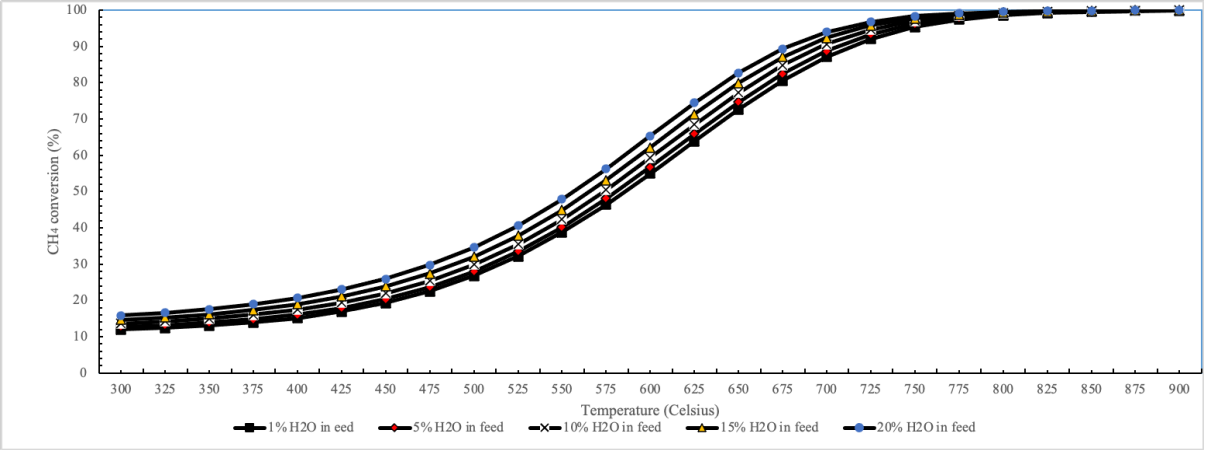

A - 28: The CH_4 conversion at varying molar fractions of H_2O in the feed

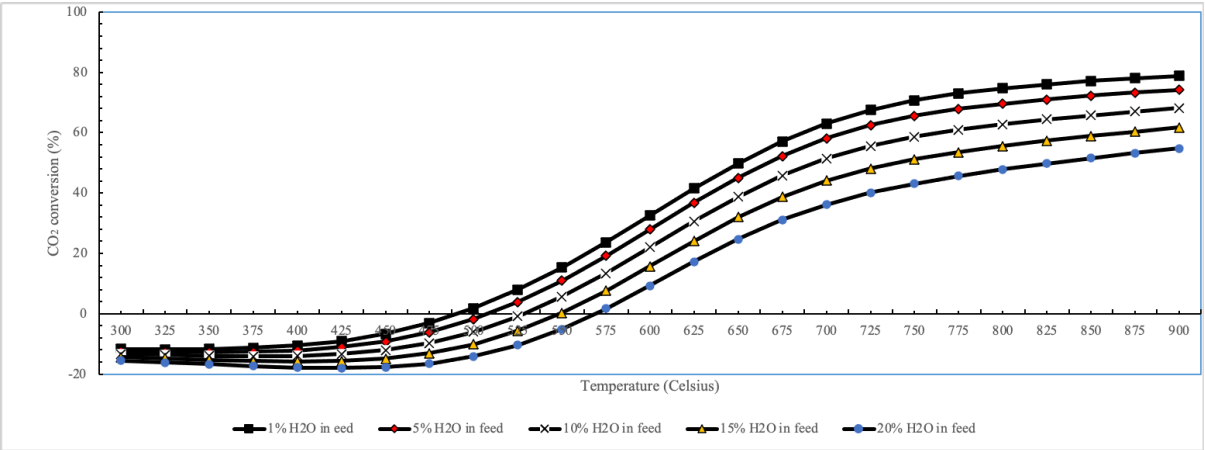

A - 29: The CO2 conversion at varying molar fractions of H2O in the feed

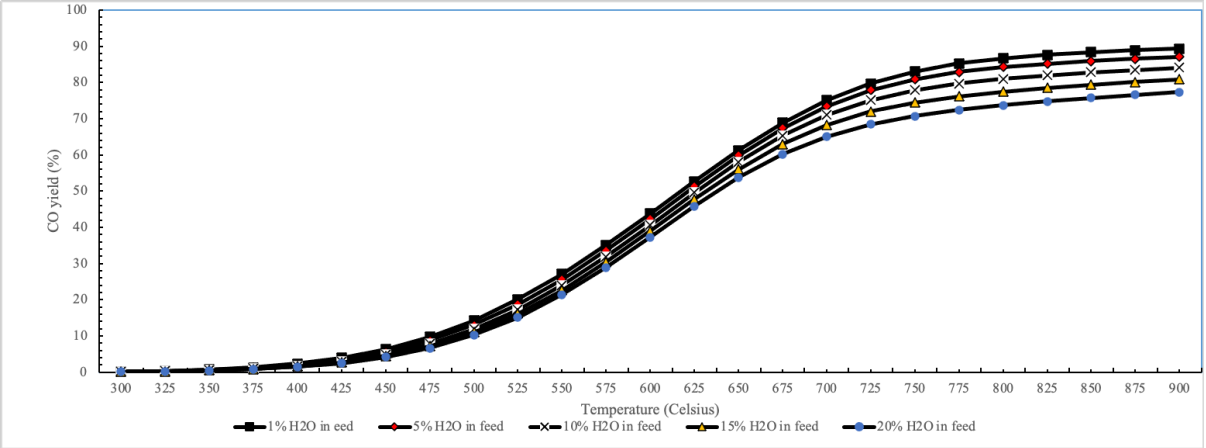

A - 30: The CO yield at varying molar fractions of H2O in the feed

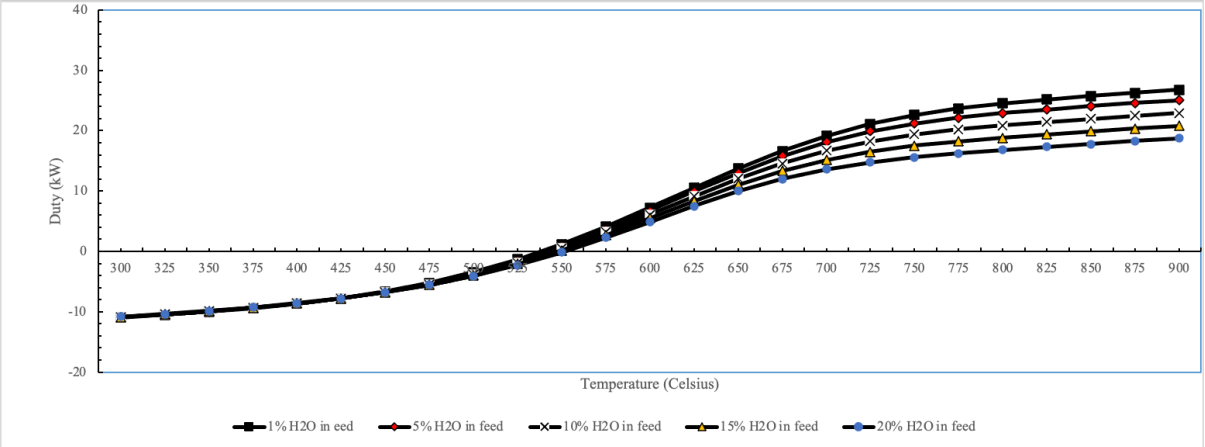

A - 31: The reactor duty at varying molar fractions of H_2O in the feed